Leaf-level metabolic changes in response to drought affect daytime CO_2 emission and isoprenoid synthesis

Running title: Drought affects daytime respiration and isoprenoid synthesis

S. Nemiah Ladd[1, 2, *], L. Erik Daber[1,*], Ines Bamberger[1, a], Angelika Kübert[1, b], Jürgen Kreuzwieser[1], Gemma Purser[3, 4], Johannes Ingrisch[1, 5], Jason Deleeuw[6], Joost van Haren[6, 7], Laura K. Meredith[6, 8], Christiane Werner[1]

[1] Ecosystem Physiology, Albert-Ludwigs-University of Freiburg, Georges-Köhler-Allee 053/054, 79110 Freiburg, Germany

[2] Department of Environmental Sciences, University of Basel, Bernoullistrasse 30, 4056 Basel, Switzerland

[3] School of Chemistry, The University of Edinburgh, Joseph Black Building, David Brewster Road, Edinburgh, EH9 3FJ, UK

[4] UK Centre for Ecology & Hydrology, Bush Estate, Penicuik, EH26 0QB, U K

[5] Department of Ecology, University of Innsbruck, Sternwartestrasse 15, 6020 Innsbruck, Austria

[6] Biosphere 2, University of Arizona, 32540 S. Biosphere Rd., Oracle, AZ, 85739, USA

[7] Honors College, University of Arizona, 1101 E. Mabel Street, Tucson, AZ, 85719, USA

[8] School of Natural Resources and the Environment, University of Arizona, Tucson, AZ, USA

*Equal contributions

[a] Current address: Atmospheric Chemistry Group, University of Bayreuth (BayCEER), Dr-Hans-Frisch-Straße 1-3, 95448 Bayreuth, Germany

[b] Current address: Institute for Atmospheric and Earth System Research, University of Helsinki, Pietari Kalmin katu 5, 00014 Helsinki, Finland

Email addresses: n.ladd@unibas.ch, erik.daber@cep.uni-freiburg.de, i.bamberger@mail.de, angelika.kuebert@mail.cep.uni-freiburg.de, juergen.kreuzwieser@ctp.uni-freiburg.de. gepurse25@ceh.ac.uk, Johannes.Ingrisch@uibk.ac.at, jdeleeuw@arizona.edu, jvanhare@arizona.edu, laurameredith@arizona.edu, c.werner@cep.uni-freiburg.de

Date submitted: 29. April, 2022
Figures: 8
Tables: 1
Word count: 4466

Highlight: Intracellular carbon allocation into daytime respiration and VOCs is species-specific and changes with drought. Isoprenoid synthesis in the plastid can be fed with glyceraldehyde-3-phosphate and geranyl pyrophosphate from the cytosol.

Abstract

Daytime respiration in leaves is an integral component of plant metabolism, with CO_2 produced as a byproduct during the synthesis of many secondary metabolites, including many common volatile organic compounds (VOCs). It remains unclear how the carbon fluxes associated with daytime respiration and VOC emission vary among mature trees, and how they are influenced by drought. We used position-specific ^{13}C-pyruvate labeling to investigate CO_2 and VOC fluxes from the leaves of four tropical species before and during an artificially imposed drought in an enclosed rainforest. Although daytime respiration was always dominated by non-mitochondrial processes, the relative contribution of CO_2 from the tricarboxylic acid cycle increased under drought, likely due to osmolyte production. In the legume tree *Clitoria fairchildiana*, our data indicate that intermediates from the mevalonic acid pathway are used to produce the volatile monoterpene trans-β-ocimene, but not isoprene. This suggests that geranyl pyrophosphate is the more important intermediate for crosstalk between cytosolic and plastidic isoprenoid synthesis, not isopentenyl pyrophosphate. Crosstalk declined with drought, and although trans-β-ocimene emissions increased, they were primarily sourced from storage and not *de novo* synthesis. We found highly species-specific dynamics in carbon allocation into different metabolic processes including daytime respiration and VOC synthesis.

Key Words: crosstalk, daytime respiration, drought, isoprenoids, position-specific isotope labeling, tropical plants

Abbreviations

acetyl-CoA	acetyl coenzyme A
B2WALD	Biosphere 2 Water Atmosphere and Life Dynamics
DMAPP	dimethylallyl pyrophosphate
FEP	fluorinated ethylene propylene
GA-3-P	glyceraldehyde-3-phosphate
GABA	γ-aminobutyric acid
GC-MS-C	Gas Chromatography – Mass Spectrometry – Combustion interface
GPP	geranyl pyrophosphate
ID	inner diameter
IPP	isopentenyl pyrophosphate
IRIS	isotope ratio infrared spectrometer
IRMS	isotope ratio mass spectrometer
MVA	mevalonic acid
MEP	methylerythritol 4-phosphate
MSD	mass-selective detector
PAR	photosynthetic active radiation
PFA	perfluoroalkoxy alkane
PTR-TOF-MS	proton transfer reaction – time of flight mass spectrometer
TCA	tricarboxylic acid
VPDB	Vienna Pee Dee Belemnite
VOCs	volatile organic compounds

Introduction

Carbon flows both in and out of plant leaves, including during daylight hours when active photosynthesis results in net uptake of CO_2. Throughout the day, plants release carbon in the form of CO_2 (Atkin *et al*., 2000; Sweetlove *et al*., 2013; Tcherkez *et al*., 2017; O'Leary *et al*., 2019) and also as volatile organic compounds (VOCs) (Rasmussen, 1970; Monson and Fall, 1989; Harrison *et al*., 2013). In order to understand how net carbon uptake by plants will change under global warming, it is important to understand how the different processes by which plants release CO_2 and VOCs vary in response to environmental stresses (Niinemets *et al*., 2010; Heskel *et al*., 2013; Schimel *et al*., 2015; Wehr *et al*., 2016). For example, more frequent and/or more intense droughts are expected for many regions as the climate warms and evaporative demand increases (IPCC, 2021). It is well known that plants will take up less CO_2 under drought stress, as they reduce their stomatal conductance to conserve water (Reddy *et al*., 2004; Pinheiro and Chavez, 2011). However, the net change in carbon uptake by plants under drought will be caused not only due to reduced photosynthesis, but also to changes in respiration (Metcalfe *et al*., 2010; Zhao *et al*., 2013).

Respiration is often defined as a catabolic process, breaking down organic molecules in the mitochondria to release energy and CO_2. However, CO_2 emissions can also be anabolic, as it is released as a byproduct during the assembly of other molecules (Tcherkez *et al*., 2008; Sweetlove *et al*., 2013; O'Leary *et al*., 2019). While net respiration rates are highest during the night when photosynthesis is inhibited, daytime respiration is a significant carbon flux as well, and is made up of both catabolic and anabolic processes (Sweetlove *et al*., 2013; O'Leary *et al*., 2019). Because these processes serve different functions for the plant, it is not clear that changes in their rates would co-vary, and the relative amounts of CO_2 generated by different processes may change as the need for energy and specific metabolites shifts (Tcherkez *et al*., 2017; O'Leary *et al*., 2019).

One way to distinguish the relative importance of different sources of CO_2 production by plants is through labeling with position-specific ^{13}C-enriched central metabolites, such as glucose or pyruvate (Tcherkez *et al*., 2008; Priault *et al*., 2009; Wegener *et al*., 2010; Jardine *et al*., 2014). This approach makes use of the fact that different carbon atoms within an individual molecule will be used for distinct biochemical processes. The ^{13}C label is preferentially allocated into different products depending on which biochemical pathway the initial central metabolite follows (Werner *et al*., 2009; Tcherkez *et al*., 2012; Fasbender *et al*., 2018). For compounds like CO_2 that are produced by multiple biochemical pathways, the relative amount of ^{13}C enrichment that occurs following the introduction of different

135 position-specific labels can thus be used to determine the relative importance of different
136 production pathways (Priault *et al*., 2009; Tcherkez *et al*., 2017). In the case of CO_2, carbon
137 atoms from the C2 and C3 positions of pyruvate are only respired in the tricarboxylic acid
138 (TCA) cycle (**Figure 1, step 1**) (Tcherkez *et al*., 2005; Fasbender *et al*., 2018). ^{13}C
139 enrichment of CO_2 following labeling with ^{13}C-2-pyruvate is therefore indicative of TCA
140 cycle activity. Carbon atoms from the C1 position of pyruvate are also released due to TCA
141 cycle activity, as pyruvate is decarboxylated to form acetyl-CoA, which is fed into the TCA
142 cycle (**Figure 1**) (Priault *et al*., 2009). However, numerous anabolic processes also
143 decarboxylate pyruvate. For example, pyruvate-derived acetyl-CoA is also the building block
144 of fatty acids and of isoprenoids produced in the cytosolic mevalonic acid (MVA) pathway
145 (**Figure 1, step 5**) (Schuhr *et al*., 2003). Additionally, carbon from the C1 position is also
146 converted to CO_2 when pyruvate combines with glyceraldehyde 3-phosphate (GA-3-P) to
147 form methylerythritol phosphate (MEP) in the plastidic MEP pathway for isoprenoid
148 synthesis (**Figure 1, step 2**) (Dudareva *et al*., 2004). Together, these processes cause ^{13}C
149 enrichment of CO_2 following labeling with $^{13}C1$-pyruvate to be greater than ^{13}C enrichment
150 of CO_2 following labeling with $^{13}C2$-pyruvate during the day, when the TCA cycle is
151 downregulated (Priault *et al*., 2009; Fasbender *et al*., 2018). The relative difference in ^{13}C
152 enrichment of CO_2 following labeling with each type of pyruvate is thus broadly indicative of
153 the relative significance of CO_2 production from non-mitochondrial anabolic processes.
154 Position-specific ^{13}C labeling can also be employed to study the synthesis of various
155 plant metabolites, including VOCs, fatty acids, and sterols (Fasbender *et al*., 2018; Yáñez-
156 Serrano *et al*., 2018, 2019; Werner *et al*., 2020; Ladd *et al*., 2021). This approach can be
157 particularly helpful for understanding the biosynthesis of both volatile and non-volatile
158 isoprenoids, and for assessing the role of metabolic crosstalk between the MEP and MVA
159 pathways for isoprenoid biosynthesis (**Figure 1, step 4 & 5**) (Ladd *et al*., 2021). The
160 maintenance of two parallel pathways for isoprenoid synthesis is unique to higher plants and
161 some algae (Arigoni *et al*., 1997; Hemerlin *et al*., 2003), and it has been suggested that plants
162 use this metabolic redundancy to improve their resistance to environmental stressors via the
163 exchange of isopentenyl pyrophosphate (IPP) or other common precursors across the plastid
164 membrane (Hemerlin *et al*., 2012). The prevalence and importance of crosstalk between the
165 MEP and MVA pathways remains controversial, in part because of a lack of identified
166 transporters that can move IPP across the plastid membrane (Rasulov *et al*., 2018; Souza *et*
167 *al*., 2018). Recent studies with position-specific ^{13}C labeling demonstrate that this approach
168 can distinguish the transfer of precursor molecules between the two isoprenoid synthesis

169 pathways, and offers an opportunity to assess if these rates change with environmental
170 stressors such as heat stress and drought (Werner *et al*., 2020; Ladd *et al*., 2021).

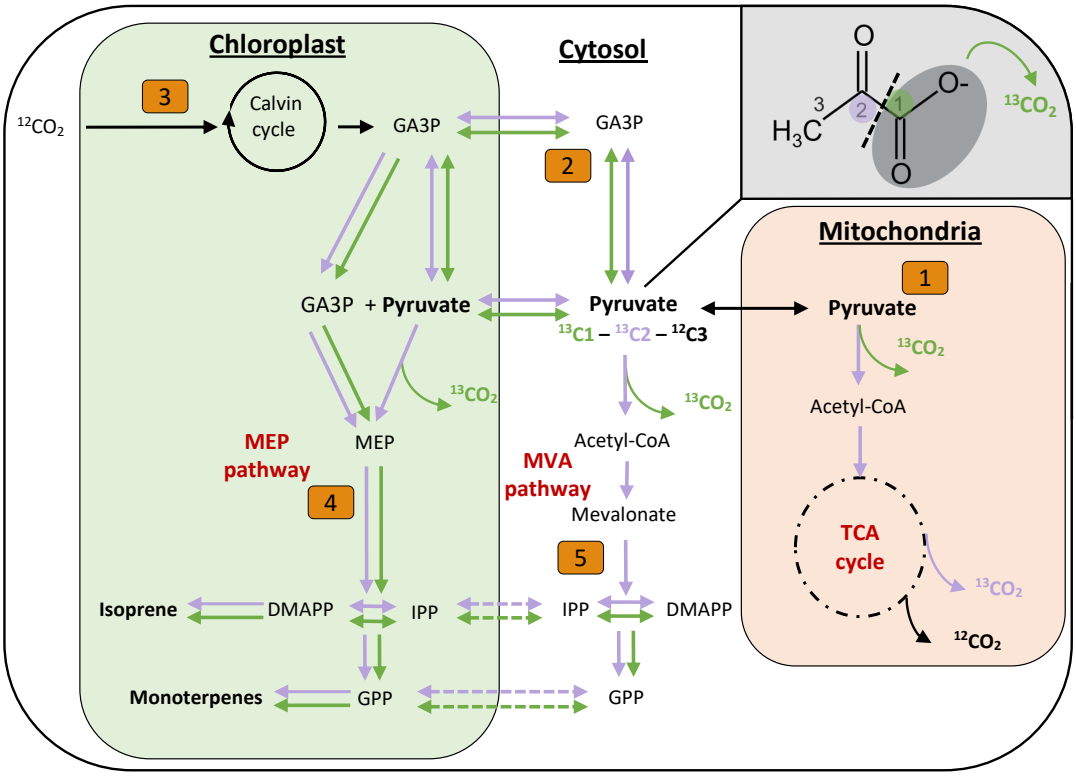

171

172 **Figure 1:** Schematic representation of important processes for the synthesis of isoprenoids and
173 production of CO_2 within plant cells, with several intermediate steps removed for clarity. Green arrows
174 represent possible movement of carbon from the C1 position of pyruvate and purple arrows represent
175 movement of carbon from the C2 position of pyruvate. Numbers represent the relevant pathways
176 discussed. 1: Transport of pyruvate into mitochondria, followed by initial decarboxylation of the C1-
177 position and entrance into the TCA-cycle (i.e., catabolic respiration). 2: Conversion of pyruvate to GA-
178 3-P and transport into the chloroplast. Pyruvate might also be transported directly to the chloroplast.
179 All carbon positions of pyruvate remain in both cases. 3: Entrance of CO_2 into the Calvin cycle and
180 addition of GA-3-P and other assimilation products into the metabolic pool of the chloroplast. 4: Initial
181 reaction of pyruvate and GA-3-P to form DMAPP and IPP via MEP pathway, followed by reaction of
182 two DMAPP/IPP molecules to produce GPP. As GA-3-P is not decarboxylated in this reaction, all
183 carbon positions of the converted GA-3-P remain in the produced isoprene and monoterpenes.
184 Pyruvate on the other hand is decarboxylated, resulting in only the C2-position remaining in these
185 products 5: Entrance of pyruvate into MVA pathway and initial decarboxylation (i.e., anabolic
186 respiration) of the C1-position of pyruvate to form DMAPP, IPP and subsequently GPP in the cytosol.
187 After transport of these metabolites incorporating the $^{13}C2$-label into the chloroplast, DMAPP and IPP
188 can either enter isoprene or monoterpene synthesis, while GPP is utilized to synthesize
189 monoterpenes. TCA, tricarboxlic acid; GA-3-P, glyceraldehyde 3-phosphate; DMAPP Dimethylallyl
190 pyrophosphate; IPP, isopentenyl pyrophosphate; MEP, methylerythritol phosphate; GPP, geranyl
191 pyrophosphate; MVA, mevalonic acid.
192

193 Previous studies that used position-specific ^{13}C labeling to learn about the production
194 of CO_2 and isoprenoids were conducted under controlled perturbations in growth chambers
195 (Tcherkez *et al*., 2005; Priault *et al*., 2009; Ghirado *et al*., 2014; Jardine *et al*., 2014;

Fasbender *et al*., 2018; Yáñez-Serrano *et al*., 2018, 2019; Werner *et al*., 2020; Ladd *et al*., 2021). These growth chamber studies have, by necessity, focused on relatively young and immature plants, and it has remained challenging to conduct a controlled experiment of this type with mature trees integrated within an ecosystem. However, there is also a need to understand how CO_2 and VOC production varies among mature plants in an ecosystem context, as this is more representative of how such fluxes respond to environmental change in nature (Guenther *et al*., 1995; Peñuelas and Staudt, 2010; Materić *et al*., 2015).

To assess the metabolic processes responsible for daytime emissions of CO_2 and volatile isoprenoids in mature plants, and to determine if these carbon fluxes change with drought stress, we used position-specific ^{13}C-pyruvate labeling to study leaf level CO_2 and VOC fluxes before and during drought in an enclosed rainforest at the Biosphere 2 research facility. We focused on fluxes from four tropical plant species, including two canopy forming trees (*Clitoria fairchildiana* and *Phytolacca dioica*) and two understory plants (*Hibiscus rosa sinensis* and a *Piper* species tentatively identified as *Piper auritum*), representing a range of functional responses to drought (Werner *et al*., 2021; Huang *et al*., in review). We calculated the amount of pyruvate label from both the C1 and the C2 position that was allocated to CO_2 and, in the case of *C. fairchildiana*, to emissions of isoprene and monoterpenes to gain insights into possible metabolic adjustments towards drought.

Materials and Methods

Drought campaign

This study took place within the context of the broader Biosphere 2 Water Atmosphere and Life Dynamics (B2WALD) campaign, described in detail by Werner *et al*. (2021). The B2WALD campaign made use of the unique thirty-year-old enclosed rainforest at the Biosphere 2 research facility, located outside Oracle, AZ, USA. In 2019, this manipulatable, mature ecosystem was subjected to a 65-day drought, with intensive monitoring of gas fluxes from leaves, stems, soils, and roots throughout a 110-day period before, during, and after drought (Werner *et al*., 2021). Under non-drought conditions, the Biosphere 2 rainforest receives 1600 mm/year, distributed by overhead sprinklers three times per week. Following the rain event on the night of 7 October 2019, we turned off the sprinkler system and did not add additional water to the system until 2 December 2019 (Werner *et al*., 2021). Daytime temperatures within the canopy of the Biosphere 2 rainforest ranged from 23.3 to 33.5 °C during the pre-drought period and 22.2 to 34.8 °C during the drought. Corresponding daytime temperature ranges for the understory were 21.3 - 26.6 °C

and 22.2 - 29.6, respectively. While there were no seasonal trends in the temperature inside the biome, maximum PAR values outside the enclosure declined from 1685 to 1016 μmol m^{-2} s^{-1} (Werner *et al*., 2021).

Plant species selection

For this study, we focused on leaf fluxes from four species in the Biosphere 2 rainforest, which were among the most abundant taxa in the forest and were selected to represent a range of drought responses and microclimates within the forest. *Clitoria fairchildiana* R.A. Howard, a large, canopy forming tree, makes up ~30 % of the forest canopy. *Phytolacca dioica* L. also represents another large canopy forming tree, and we included two large individuals as well as two smaller individuals (~10 m tall). From the understory, we included the fast-growing, herbaceous perennial from the genus *Piper*, most likely *Piper auritum* Kunth, and *Hibiscus rosa sinensis* L., an evergreen woody shrub.

Gas sampling system and analyzers

For all target species, we enclosed whole leaves in species-specific, gas-tight chambers made from FEP film wrapped around frames of copper wire enclosed in PFA tubing. One end of the leaf chamber was sealed around the petiole, while the other end was sealed around the incoming and outcoming PFA tubes. For *H. rosa sinensis*, we used larger chambers that enclosed several leaves on terminal branches. This was necessary because it was difficult to avoid embolism when cutting the petiole of single *H. rosa sinensis* leaves.

We supplied each chamber with a blend of air created from clean, VOC and CO_2-free air produced by a Zero Air Generator (Aadco Instruments, Inc., Cleves, OH, USA) and a controlled amount of CO_2 (~500 ppm, $\delta^{13}C$ ~ -10 ‰) from a gas tank. Each chamber was equipped with a fan to guarantee efficient air mixing. The outflow from the chamber was connected to a Teflon T-piece and ball valve that allowed us to sample a portion of the flow onto cartridges for offline analyses (details below). Additional flow was diverted to three analyzers: (1) a proton transfer reaction – time of flight mass spectrometer (PTR-TOF-MS 4000ultra, Ionicon Analytic, Innsbruck, Austria) that measured VOC fluxes, (2) a carbon isotope ratio infrared spectrometer (Delta Ray IRIS, Thermo Fisher Scientific, Bremen, Germany), and (3) a water isotope cavity ring-down spectrometer (L2120i water isotope analyzer, Picarro Inc., Santa Clara, CA, USA). Details of the gas sampling system, analyzers,

and the calibration of different analyzers used during the B2WALD campaign are provided in Werner et al. (2021).

Position-specific ^{13}C-pyruvate labeling

We conducted position-specific ^{13}C-pyruvate labeling during two time periods: pre-drought (12 – 28 September 2019) and drought (4 – 16 November, 2019; after 27 – 39 days without rain), using a protocol similar to that of Fasbender *et al*. (2018). For canopy trees, we did the labeling during the morning hours, when overall photosynthesis tends to be highest in the Biosphere 2 rainforest (Rascher *et al*., 2004; Rosolem *et al*., 2010). For the understory plants, we did most of the labeling in the afternoon, and tried to have the leaf in the sun for at least part of the labeling event. We installed leaf chambers at least one day prior to the labeling event. Immediately prior to labeling, we monitored the chamber for 15 minutes to ensure that leaf fluxes were stable. We then cut the leaf petiole and placed it under water, and cut it again to avoid embolism. The petiole remained in an Eppendorf tube filled with water for five more minutes so that the fluxes could stabilize after cutting. Subsequently, we exchanged the Eppendorf tube with one containing a 10 mM solution of either ^{13}C1- or ^{13}C2-pyruvate (99 atom % ^{13}C, Cambridge Isotope Laboratories, Andover, MA, USA). If most of the initial solution was taken up by transpiration during the following 80 minutes of measurements, we exchanged it with a new Eppendorf tube containing the same solution. After 80 minutes, we removed the Eppendorf tubes and weighed them. We used the change in mass relative to the pre-measurement mass to calculate the mass of label uptake.

We collected the leaf after each measurement to determine its leaf area by tracing it on a sheet of paper of known mass and weighing the leaf's shape on a fine mass-balance. We filled missing leaf area values with the median value of all leaves of the same species (n = 16).

Cartridge sampling and analyses

During each pyruvate labeling event, we also collected VOCs on glass cartridges filled with Tenax. We used an air sampling pump (220-1000TC, SKC, Eighty Four, PA, USA) to maintain a defined air flow (100 - 200 ml min^{-1}) through the cartridge. We attached the cartridges to the chamber for at least 30 minutes prior to the leaf cutting and for ~70 minutes of the 80 minutes that the leaf petiole was submersed in the pyruvate solution. Parallel to the collection of each plant chamber cartridge, we collected a cartridge from the empty cuvette to correct for chamber background and other contaminants. After sample

collection we sealed the cartridges in vacutainers and stored them at room temperature prior to analysis.

We subsequently analyzed all cartridge samples by Gas Chromatography – Mass Spectrometry – Combustion interface – Isotope Ratio Mass Spectrometry (GC-MS – C – IRMS) to identify and quantify the emitted VOCs and to determine the $\delta^{13}C$ values of individual VOCs. Volatiles were analyzed after thermodesorption on a gas GC (7890B, Agilent Technologies Böblingen, Germany) equipped with a mass-selective detector (MSD, 5975C, Agilent Technologies Böblingen, Germany) and a thermodesorption/cold injection system (TDU-CIS4, Gerstel, Germany). VOCs were desorbed from cartridges at 220 °C and immediately trapped in the CIS at −70°C. The CIS was heated up to 240 °C, channeling the volatiles onto the separation column (DB-5ms UI, 30 m × 0.25 mm ID, 0.25 µm film thickness, Agilent Technologies Böblingen, Germany). Further details on GC oven and MSD settings are given by Haberstroh *et al*. (2018). To quantify specific compounds (i.e., main monoterpenes including trans-β-ocimene), we regularly analyzed calibration curves with authentic standards. We analyzed chromatographic raw data with MassHunter Software (Agilent Technologies Böblingen, Germany). We compared mass spectra with the NIST mass spectral library and the retention times of authentic standards to identify compounds of interest.

10 % of the column effluent was diverted to the MSD by a splitter at the end of the GC column, while the remainder of the sample was transferred to an Isotope Ratio Mass Spectrometer (IRMS; Isoprime precisION, Elementar, Hanau, Germany) via a combustion furnace (GC5 interface, Elementar, Hanau, Germany). The latter was operated at 850 °C and combusted VOCs with CuO to CO_2 and water. After removal of water by a Nafion trap, the CO_2 was directed into the continuous flow IRMS to analyze compound specific $\delta^{13}C$ values. We regularly analyzed octane ($\delta^{13}C$: −31.75 ± 0.01 ‰) and octadecane ($\delta^{13}C$: −32.70 ± 0.01 ‰) (available from Schimmelmann lab, Indiana University, https://arndt.schimmelmann.us/compounds.html) as isotopic reference standards throughout the measurement window. We analyzed raw data with the IonIOS software (Elementar Analysensysteme GmbH, Langenselbold, Germany).

Calculations

We calculated the transpiration rate E [mmol $m^{-2}s^{-1}$] and the assimilation rate A [µmol $m^{-2}s^{-1}$] from the concentration of water vapour and CO_2 entering and exiting the leaf cuvette

as in von Caemmerer and Farquahar (1981). We calculated instantaneous water use efficiency WUE_i [μmol CO_2/mmol H_2O] as the ratio A/E.

The Delta Ray calculated $\delta^{13}C$ values of CO_2 relative to the Vienna Pee Dee Belemenite (VPDB) scale using two internal reference gases ($\delta^{13}C$ values = -9.86 ‰ and -27.8 ‰). We calculated the ^{13}C enrichment of CO_2 ($\varepsilon^{13}C_{CO2}$) leaving the leaf chambers following labeling with ^{13}C-pyruvate as

$$\varepsilon^{13}C_{CO2} = \left(\frac{\delta^{13}C_{CO2o} + 1000}{\delta^{13}C_{CO2e} + 1000} - 1\right) * 1000 \quad (1)$$

where $\delta^{13}C_{CO2o}$ and $\delta^{13}C_{CO2e}$ are the $\delta^{13}C$ values of CO_2 exiting and entering the chamber, respectively.

We converted $\delta^{13}C$ values to the fraction of ^{13}C ($^{13}F = {}^{13}C/({}^{12}C + {}^{13}C)$) using the definition of $\delta^{13}C$ and the known $^{12}C/^{13}C$ ratio of VPDB (Hayes, 2004). We then used isotopic mass balance to determine the net isotopic effect of photosynthesis and respiration on the ^{13}F value of CO_2 leaving the leaf chamber, $^{13}F_{CO2}$, prior to labeling as:

$$^{13}F_P = \frac{c_e * {}^{13}F_e - c_o * {}^{13}F_o}{c_e - c_o} \quad (2)$$

Where $^{13}F_e$ and $^{13}F_o$ are the ^{13}F values for CO_2 and c_e and c_o are the concentrations of CO_2 at the entrance and outlet of the leaf chamber, respectively. We averaged $^{13}F_P$ values for all measurements of each species, and assumed that it remained constant throughout the pyruvate labeling event. Although this was not strictly true, the natural isotope effect of photosynthesis and respiration on the $\delta^{13}C$ value of the CO_2 leaving the chamber was relatively small (always less than 10 ‰) relative to the impact of the ^{13}C pyruvate label.

We were then able to calculate the concentration of ^{13}C originating from the pyruvate label, c_I, through isotopic mass balance as:

$$c_I = \frac{c_o * (F_o - F_P) + c_e * (F_P - F_e)}{F_I} \quad (3)$$

where the ^{13}F value of the 99 atom % ^{13}C-pyruvate label, F_I, is 0.99. We converted c_I to moles of CO_2 using the ideal gas law and the flow rate of air to the leaf chambers, and to grams of CO_2 using the molar mass of CO_2. We then compared this mass to the total mass of ^{13}C taken up from the pyruvate label to determine the percent of pyruvate carbon that was allocated to CO_2.

VOC fluxes V_l in [$nmol$ $m^{-2}s^{-1}$] were calculated from molar flow, the leaf area, the concentration of the VOC from the outlet of the empty cuvette v_e [ppb], and the concentration of the VOC at the outlet of the leaf cuvette v_o [ppb] as:

$$V_l = \frac{u}{s} * (v_o - v_e) \quad (4)$$

To distinguish VOCs that were synthesized directly from introduced ^{13}C1- or ^{13}C2-pyruvate, $^{13}V_l$, and VOCs produced only with ^{12}C, $^{12}V_l$, we calculated the fraction of the fluxes of mass 69.0683 in relation to mass 70.0719 for isoprene and mass 137.141 in relation to mass 138.145 for monoterpenes. We subsequently subtracted the theoretical value of the contribution of the heavier isotope under natural abundance of ^{13}C (1.1%) in the atmosphere $^{13}F_{na}$ (isoprene: 5.5%; monoterpenes: 11%) to calculate the excess ^{13}C fraction $^{13}F_{Vl}$ in percent.

$$^{13}F_{Vl} = \frac{^{13}V_l}{^{13}V_l + {}^{12}V_l} * 100 - {}^{13}F_{na} \quad (5)$$

To calculate ^{13}C enrichment of individual monoterpenes measured by GC-IRMS, we calculated ε^{13}C values between the δ^{13}C value of the compound during a specific labeling event and the mean δ^{13}C value of the same compound from unlabeled leaves during the same experimental phase (pre-drought or drought).

Statistics

Changes in transpiration, assimilation, leaf water potential, VOC fluxes, and ^{13}C-enrichment of CO_2 between pre-drought and drought measurements were compared for each species using Welch's t test. Differences in these variables among species were assessed with Brown-Forsyth and Welch ANOVA tests. All statistical analyses were performed in GraphPad Prism software. We used 15-minute averages from the end of the experiment (minute 55-70 after label application) for all statistical analysis and for data shown in figures.

Results

Changes in transpiration, assimilation, and leaf water use efficiency

For all species besides *H. rosa sinensis*, transpiration and assimilation rates declined during the drought (**Figure 2**). *P. dioca* displayed the highest intraspecies variability in these fluxes, with very high values observed for the leaves of the largest individual, located on the south side of the biosphere, which received more direct sunlight than the trees on the north side. *C. fairchildiana* displayed the largest relative reductions in transpiration and

assimilation, with a relatively greater decline in assimilation. *C. fairchildiana* had the highest water use efficiency of any species in both phases of the experiment, but was the only species with a significant decrease in this value during the drought (**Figure 2**).

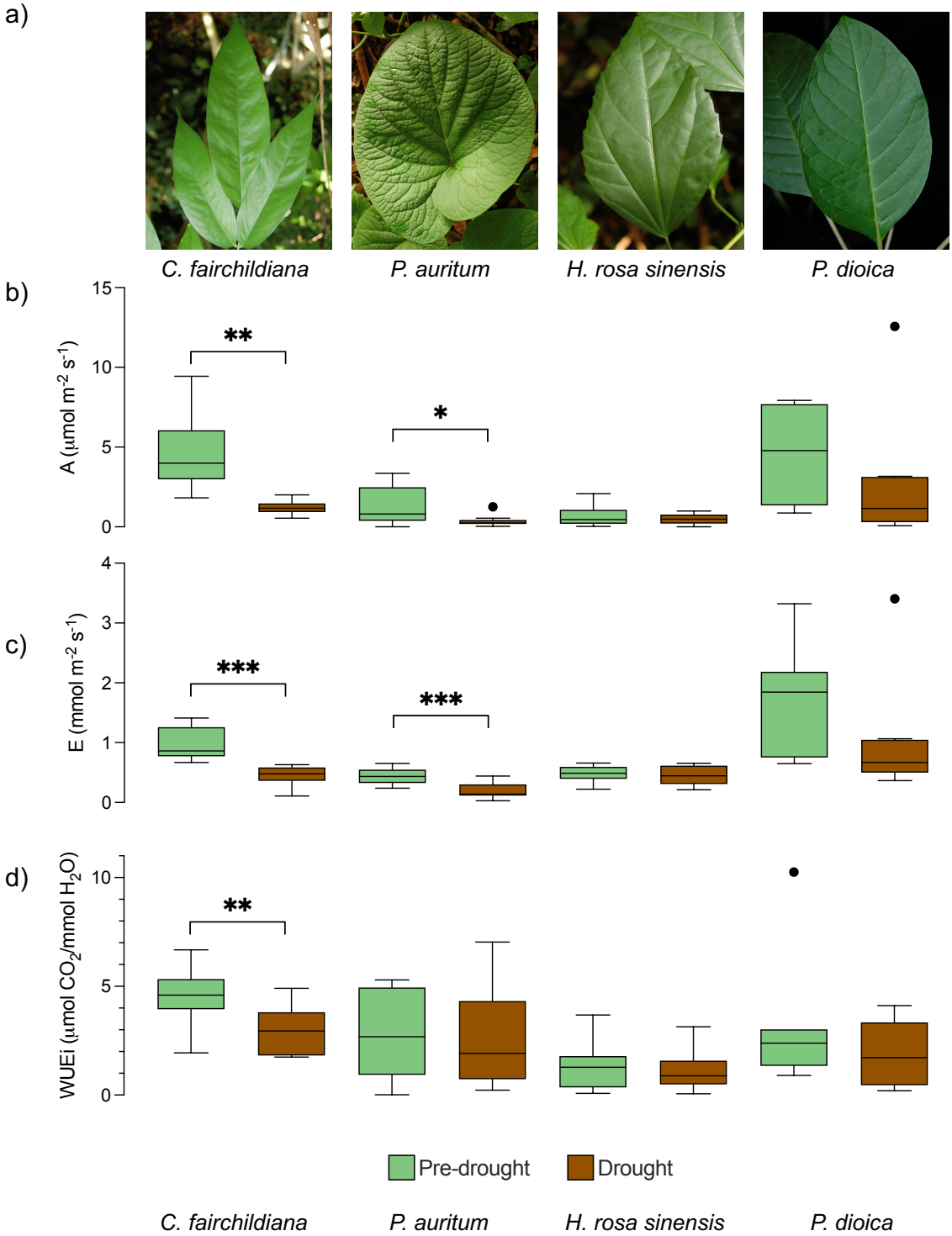

Figure 2: Representative leaves (panel a) and rates of (b) carbon assimilation, (c) transpiration, and (d) instantaneous water use efficiency measured on individual leaves of *Clitoria fairchildiana*, *Piper auritum, Hibiscus rosa sinensis*, and *Phytolacca dioica* under pre-drought (green) and drought (brown) conditions. Boxes represent the median and 25 – 75 % range of 7-12 replicate leaves. Whiskers and outliers calculated using Tukey's method. Significant differences between pre-drought

and drought conditions for each species are indicated as * when $p < 0.05$, ** when $p < 0.01$, and *** when $p < 0.001$.

VOC fluxes

C. fairchildiana had the highest isoprene fluxes of any species under both pre-drought (mean and standard error = 7 ± 3 nmol m^{-2} s^{-1}) and drought (1.1 ± 0.9 nmol m^{-2} s^{-1}) conditions (**Figure 3**). *P. auritum* had the second highest isoprene fluxes, but these were an order of magnitude lower than those from *C. fairchildiana* (0.1 ± 0.04 nmol m^{-2} s^{-1} under pre-drought conditions and ($1*10^{-4} \pm 9*10^{-5}$ nmol m^{-2} s^{-1} under drought conditions; **Figure 3**). Isoprene emissions from *H. rosa sinensis* and *P. dioica* were one to two orders of magnitude lower than those from *P. auritum*. Between the pre-drought and drought, isoprene emissions only declined significantly for *P. auritum* ($p < 0.05$), but there was declining tendency in emissions for *C. fairchildiana* and *P. dioica* as well (**Figure 3**), coincident with an overall decline in atmospheric isoprene abundance (Werner *et al*., 2021).

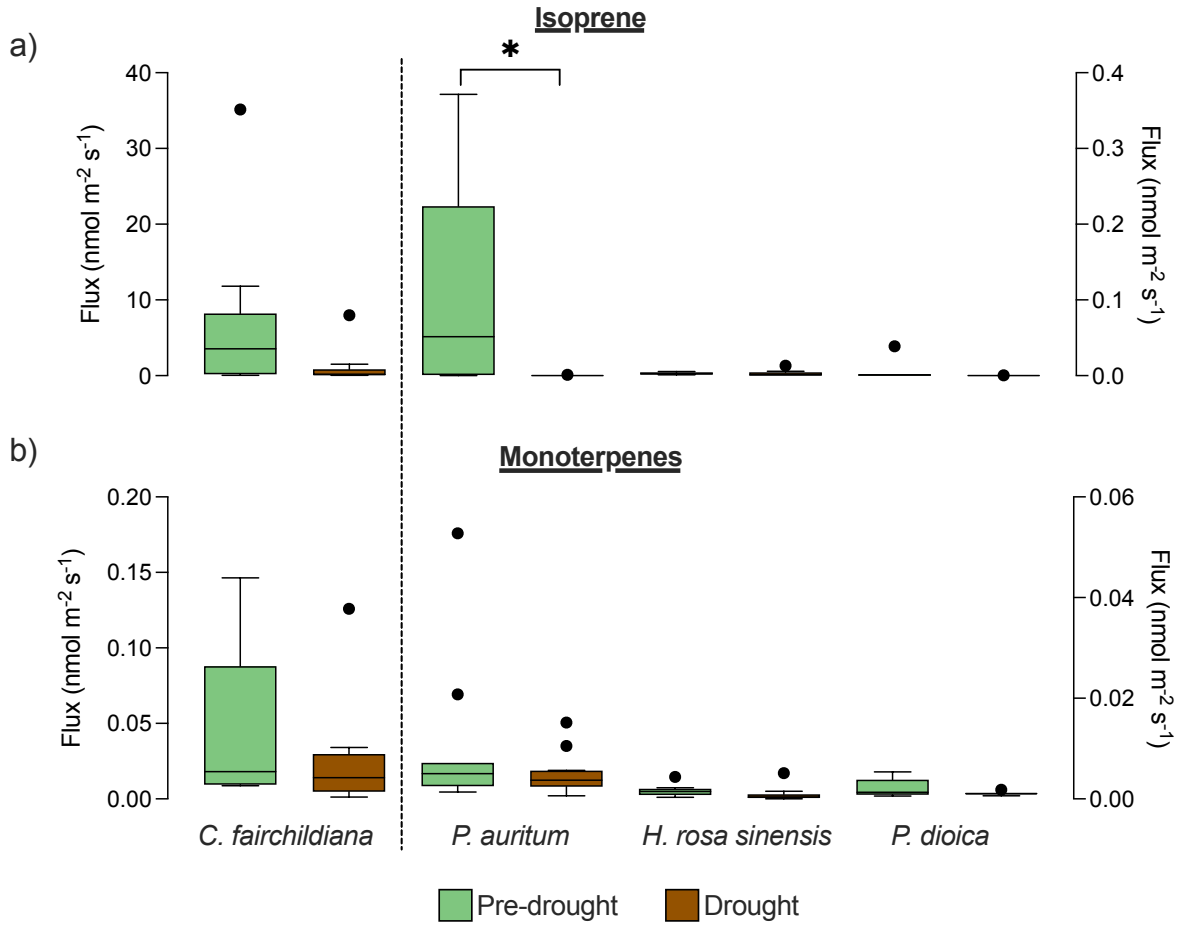

Figure 3: Emission rates of (a) isoprene and (b) monoterpenes measured on individual leaves of *Clitoria fairchildiana*, *Piper auritum, Hibiscus rosa sinensis*, and *Phytolacca dioica* under pre-drought (green) and drought (brown) conditions. Fluxes from *C. fairchildiana* are plotted on the left y-axis while all other species are plotted on the right y-axis. Boxes represent the median and 25 – 75 % range of

7-12 replicate leaves. Whiskers and outliers are calculated using Tukey's method. Significant differences between pre-drought and drought conditions for each species are indicated as: * when $p < 0.05$.

Monoterpene emissions were also at least an order of magnitude higher from *C. fairchildiana* than any other species (**Figure 3**). However, monoterpene emissions from *C. fairchildiana* were two orders of magnitude lower than isoprene emissions. The mean monoterpene emissions were lower for all species under drought conditions than under pre-drought (**Figure 3**), but not significantly. In this case, the apparent trends in the leaf fluxes diverge from the observed dynamics of monoterpenes in the atmosphere, which increased between our pre-drought and drought measurements (Werner *et al*., 2021). Analysis of cartridge samples by GC-MS (which is able to chromatographically resolve different monoterpenes) indicated that α-pinene, β-pinene, 3-carene, limonene, and trans-β-ocimene were the most abundant monoterpenes emitted by *C. fairchildiana* (**Table 1**). Fluxes of most of these compounds declined with drought, but trans-β-ocimene emissions increased by a factor of four (**Table 1**).

Table 1: Fluxes of common monoterpenes emitted by *q* as determined by GC-MS analysis of cartridge samples. Fluxes are reported as mean and standard error. [1]These two compounds co-eluted on the GC and the combined flux is reported.

	Pre-drought flux (pmol m^{-2} s^{-1})		Drought flux (pmol m^{-2} s^{-1})	
α-pinene	6.51	± 2.41	3.09	± 0.20
d-3-carene/ β-pinene[1]	9.28	± 2.96	5.52	± 0.46
limonene	5.10	± 0.79	4.39	± 0.23
trans-β-ocimene	5.47	± 1.20	28.88	± 7.35

^{13}C-enrichment of CO_2 from pyruvate

All studied plants in Biosphere 2 displayed the expected pattern of more ^{13}C-enriched CO_2 following labeling with ^{13}C1-pyruvate than with ^{13}C2-pyruvate (**Figures 4, 5**). As much as ~10 % of the total ^{13}C from the ^{13}C1-pyruvate was respired during the relatively short period of our measurement, in contrast to less than 1.5 % of the total ^{13}C taken up from the ^{13}C2-pyruvate (**Figure 4**). However, the magnitude of this difference tended to be less

pronounced for *C. fairchildiana* and *P. auritum* than for *H. rosa sinensis* and *P. dioica* (**Figures 4, 5)**. This difference is apparent by plotting the $\varepsilon^{13}C_{CO2}$ values from ^{13}C1-pyruvate labeling relative to those from ^{13}C2-pyruvate labeling, where the values for *C. fairchildiana* and *P. auritum* plot much closer to the 1:1 line than the other species do (**Figure 5**). During drought, the $\varepsilon^{13}C_{CO2}$ values during labeling with both pyruvate labels tended to decline for both *C. fairchildiana* and *P. auritum*, while for *P. dioica* they only tended to decline for labeling with ^{13}C1-pyruvate and for *H. rosa sinensis* they did not change (**Figure 5**).

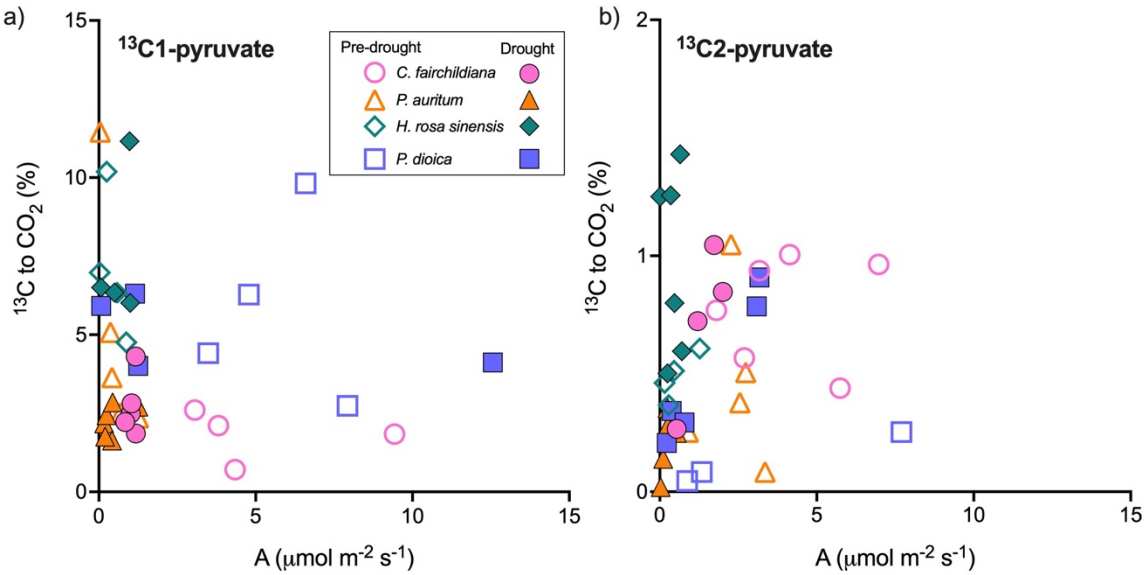

Figure 4 Percent of ^{13}C from (a) ^{13}C1-labeled pyruvate and (b) ^{13}C2-labeled pyruvate that was released as CO_2 due to day respiration by *Clitoria fairchildiana*, *Piper auritum, Hibiscus rosa sinensis*, and *Phytolacca dioica* under pre-drought (open symbols) and drought (closed symbols) conditions. Note that the y-axes differ between panels, which was necessary to distinguish changes in production of CO_2 from ^{13}C2-labeled pyruvate, which are an order of magnitude lower than those from ^{13}C1-labeled pyruvate.

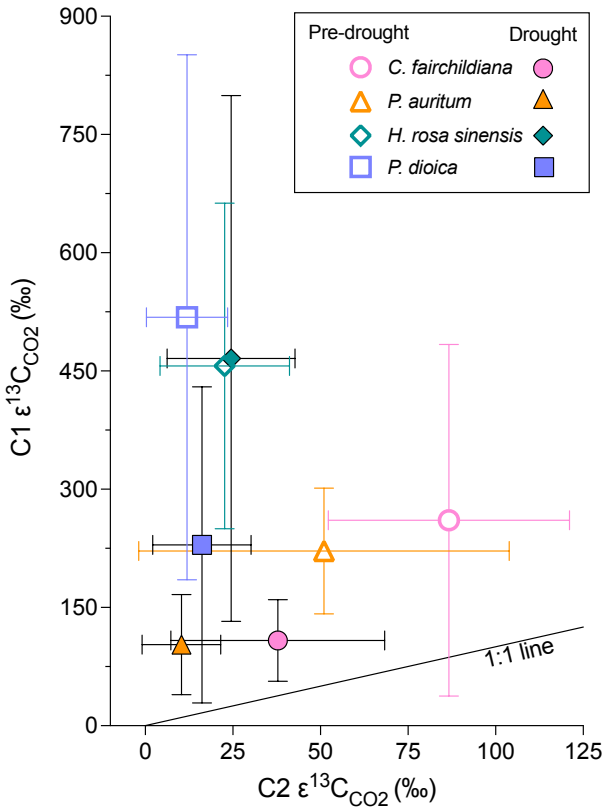

Figure 5 ^{13}C enrichment of CO_2 from $^{13}C1$-labeled pyruvate (y-axis) plotted relative to ^{13}C enrichment of CO_2 from $^{13}C2$-labeled pyruvate (x-axis) during pre-drought (open symbols) and drought (closed symbols). Symbols represent mean values and error bars represent one standard deviation of 3 – 6 replicate leaves per species.

^{13}C-enrichment of VOCs following pyruvate and CO_2 labeling limited to isoprenoids from C. fairchildiana

For most compounds from most species, ^{13}C from the pyruvate label was not incorporated at rates high enough for the ^{13}C isotopologue to be reliably detected by the PTR-TOF mass spectrometer. For VOCs that were only emitted in low quantities, it is impossible to say whether or not some of these compounds were labeled, but with a signal below the limit of detection by the mass spectrometer.

The only compounds that were clearly enriched in ^{13}C following the ^{13}C-pyruvate labeling were isoprene and monoterpenes from *C. fairchildiana*. For isoprene, ^{13}C incorporation rates were high enough that mass 70.07 (that is, isoprene molecules with a single ^{13}C atom) was sufficiently high to be reliably quantified relative to mass 69.07 (isoprene molecules with only ^{12}C), and up to 15 % of the isoprene flux was labeled with ^{13}C above the theoretical background level (**Figure 6a**), indicating that a sizable amount of isoprene was freshly synthesized from pyruvate. During pre-drought conditions, there was not a significant difference in the incorporation of ^{13}C into isoprene fluxes from the $^{13}C1$- and

^{13}C2-pyruvate labels (**Figure 6a**). Similarly, under drought, there was no significant difference in ^{13}C incorporation between the two types of labels. However, drought increased ^{13}C-isoprene emission from ^{13}C1-pyruvate ($p < 0.05$). The median ^{13}C flux of isoprene when labeled with ^{13}C2-pyruvate was similarly higher during the drought, but this increase was not significant (**Figure 6a**).

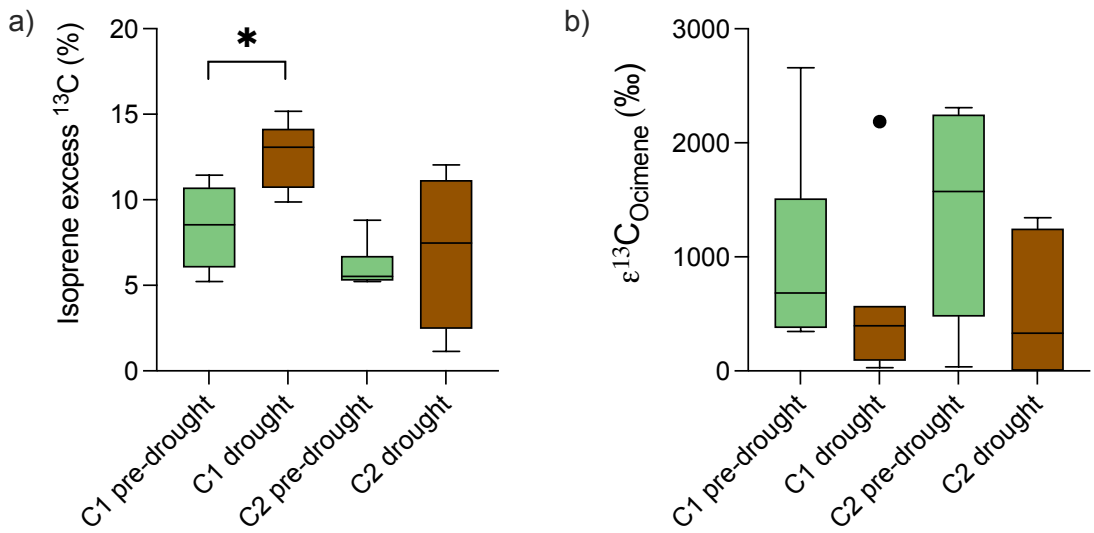

Figure 6: ^{13}C from ^{13}C-labeled pyruvate incorporation into VOCs from *Clitoria fairchildiana*. Panel (a) shows ^{13}C excess isoprene emissions relative to theoretical background levels for isoprene and (b) shows ^{13}C enrichment of the monoterpene trans-β-ocimene relative to unlabeled measurements during pre-drought (green) and drought (brown) conditions (4 – 6 replicates per treatment). Boxes represent the median and 25-75% range of 7-12 replicate leaves. Whiskers and outliers are calculated using Tukey's method.

Due to lower emissions under drought, the ^{13}C isotopologue of monoterpenes was difficult to quantify as there was excessive scatter in the measured flux. We therefore opted to assess ^{13}C incorporation into monoterpenes using the GC-IRMS data, which is able to resolve very small differences in the relative amount of ^{13}C. Of the monoterpenes collected on the cartridge samples from *C. fairchildiana*, only trans-β-ocimene became strongly enriched in ^{13}C following labeling by either type of pyruvate, with relatively more ^{13}C enrichment from ^{13}C2-pyruvate than from ^{13}C1 (**Figure 6b**). Under drought, trans-β-ocimene ^{13}C enrichment was similar from both pyruvate labels, and there was a tendency for the ^{13}C enrichment to be lower than during pre-drought (**Figure 6b**).

Discussion

During the first four weeks of drought in the Biosphere 2 rainforest, surface soil moisture was almost completely depleted and the atmospheric vapor pressure gradient

increased in both the canopy and the understory, but at a higher rate in the canopy (Werner *et al*., 2021). Drought responses among individuals of the same species were variable and impacted by microclimate conditions (**Figure 2**) (Werner *et al*., 2021). Nevertheless, clear differences in overall drought responses emerged among the four species (**Figure 7**). In the following discussion, we consider how these drought responses relate to changes in daytime respiration patterns for each species. Daytime respiration processes in *C. fairchildiana* were most distinct from the other three species (**Figures 4, 5**). For this species, we further investigate pyruvate allocation into volatile isoprenoids (**Figure 6**), and assess the role metabolic crosstalk between the MVA and MEP pathways has on the synthesis of these compounds under both pre-drought and drought conditions (**Figure 8**).

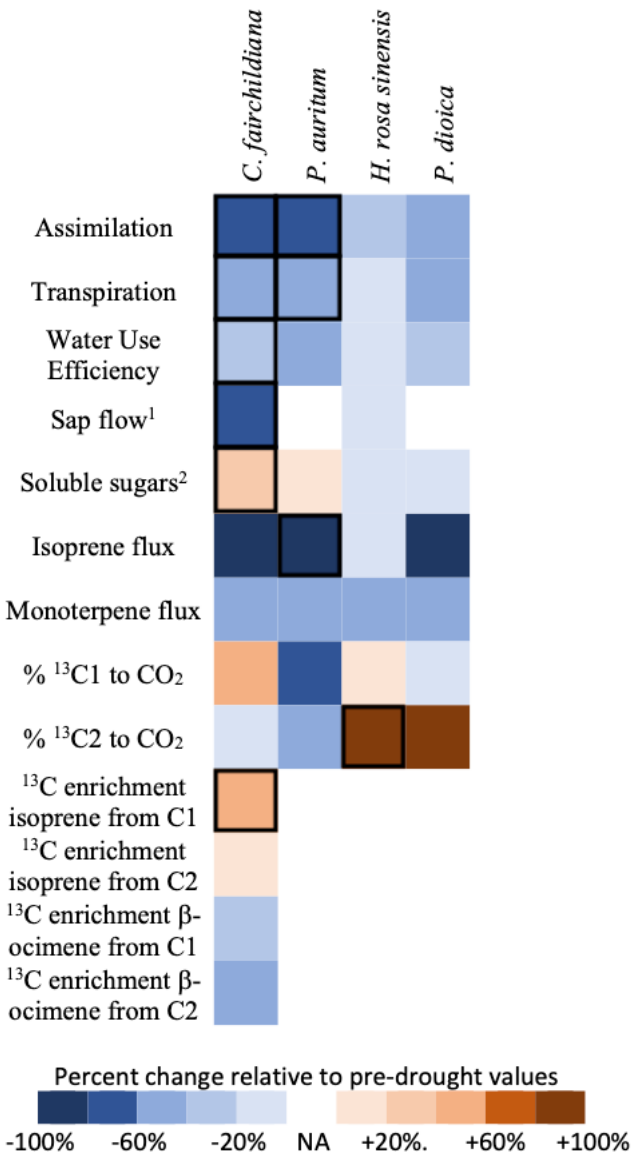

Figure 7: Trends in response to drought by *C. fairchildiana*, *P. auritum*, *H. rosa sinensis*, and *P. dioica*, expressed as percent decrease (blue shades) or increase (brown shades) of the mean drought value relative to the mean pre-drought value. Black borders indicate measurements where the mean

518 values were significantly different at the $p < 0.05$ level. [1] Data from Werner *et al*., 2021. [2] Data from
519 Huang *et al*., in review.
520

521 *Daytime CO_2 production and relationship to drought status*

522 Among the four species we studied, gas fluxes from *H. rosa sinensis* were least
523 affected by drought, with leaf level assimilation and transpiration rates remaining relatively
524 consistent (**Figures 2, 7**). These rates were quite low both before and during drought, and
525 these understory shrubs may have been light limited throughout the entire time period. *H.*
526 *rosa sinensis* displayed the expected pattern of ^{13}C enrichment of CO_2 when supplied with
527 position-specific ^{13}C-pyruvate: ^{13}C from the C1 position of pyruvate was rapidly respired,
528 while the C2 position was not (**Figures 4, 5**) (Priault *et al*., 2009; Werner *et al*., 2009). This
529 indicates an inhibited TCA cycle, but ample CO_2 production from anabolic processes.
530 However, TCA cycle activity, as evidenced by ^{13}C enrichment of CO_2 during $^{13}C2$-pyruvate
531 labeling, increased with drought, and reached higher levels than those observed for any other
532 species (**Figure 4**). This increased TCA cycle activity could represent an early drought
533 response by *H. rosa sinensis*, as it is associated with elevated synthesis of amino acids such
534 as L-glutamate. L-glutamate is produced in the TCA cycle and is the direct precursor for the
535 osmoregulatory solute proline (Delauney and Verma, 1993), which starts to accumulate in
536 plant cells under drought (Shinozaki and Yamaguchi-Shinozaki, 1998; Farooq *et al*., 2012).
537 Consistent with this speculation, the roots of *H. rosa sinensis* had pronounced accumulation
538 of osmolytes during the B2WALD drought and upregulated synthesis of γ-aminobutyric acid
539 (GABA) (Honneker *et al*., 2022), which can stimulate accumulation of proline (Nayyar *et al*.,
540 2014).

541 Even though overall assimilation and transpiration rates did not decline significantly
542 for *P. dioica* under drought, all trees except for the largest individual on the south side of the
543 Biosphere 2 rainforest experienced a visible decline in these rates (**Figure 2**). Although gas
544 exchange rates in *P. dioica* tended to be more affected by the drought than in *H. rosa*
545 *sinensis*, the two species displayed similar trends in their rates of CO_2 emission before and
546 during the drought. Just like *H. rosa sinensis*, *P. dioica* allocated a similar percent of ^{13}C
547 from $^{13}C1$-pyruvate to anabolic daytime respiration before and during drought, demonstrating
548 the importance of maintaining metabolic activities that result in the release of CO_2 even as
549 overall carbon availability tended to decline (**Figure 4**). Likewise, there was a tendency for
550 TCA cycle activity to increase, as most leaves respired more ^{13}C from $^{13}C2$-pyruvate during
551 the drought (**Figure 4**).

552 In comparison with *H. rosa sinensis* and *P. dioica*, *P. auritum* was much more visibly
553 affected after a month of drought, with significant reductions in both assimilation and
554 transpiration (**Figures 2, 7**). Before the drought, all three species decarboxylated similar
555 amounts of ^{13}C from $^{13}C1$-pyruvate, but this allocation declined by 56 % for *P. auritum*
556 during the drought (**Figure 4**). This reduction in anabolic CO_2 production was independent of
557 the decline in gas exchange rates, since none of the leaves used for labeling with $^{13}C1$-
558 pyruvate had high assimilation rates during the pre-drought measurements (**Figure 4**),
559 perhaps because of relatively low light levels. In contrast to *P. dioica* and *H. rosa sinensis*,
560 the percent of respired $^{13}C2$-pyruvate tended to decline in *P. auritum* leaves, and may have
561 been indicative of the more advanced drought stress experienced by this species (**Figures 4,**
562 **7**). These adjustments suggest a concurrent decline in daytime respiration from mitochondrial
563 and non-mitochondrial processes, which may have been due to less metabolic activity.
564 Additionally, amino acids may not have been used as significant osmolytes in *P. auritum*
565 leaves, which were characterized by an accumulation of soluble sugars (**Figure 7**; Huang *et*
566 *al*., in review), which can also help maintain cell turgor by decreasing osmotic potential
567 (Anjum *et al*., 2011; Farooq *et al*., 2012; Bhargava and Sawant, 2013). The dominant
568 osmolytes produced by a plant may thus affect its CO_2 production under drought, with
569 daytime respiration enhanced in plants that tend to rely on amino acids rather than sugars.
570 *C. fairchildiana* displayed the strongest responses to drought, with significant
571 reductions in assimilation, transpiration, and water use efficiency (**Figures 2, 7**). At the same
572 time, *C. fairchildiana* displayed significant structural responses to the drought, shedding ~ 25
573 % of its leaves, which, along with reduced transpiration rates at the level of individual leaves,
574 resulted in an 76 % reduction in sap flow (Werner *et al*., 2021; Huang *et al*., in review). At
575 the same time however, *C. fairchildiana* was the only species in which no changes in the
576 percent of $^{13}C1$ and $^{13}C2$-pyruvate converted to CO_2 were observed, even though, like *P.*
577 *auritum*, it upregulated its concentration of leaf-soluble sugars (**Figure 7**; Huang et al., in
578 review). Although both *P. auritum* and C. *fairchildiana* decarboxylated similarly low
579 amounts of $^{13}C1$-pyruvate under drought (**Figure 4**), the low rates observed for C.
580 *fairchildiana* are unlikely to be driven by its drought-induced declines in assimilation, as the
581 percentage of ^{13}C-pyruvate that was respired was unchanged from pre-drought conditions,
582 when both assimilation and transpiration rates were high. This suggests that the mechanism
583 responsible for low anabolic daytime respiration by *C. fairchildiana* is not related to the
584 drought, and therefore different from the mechanism that caused *P. auritum*'s daytime CO_2
585 production to decline with drought.

586

587 *Metabolic link between MEP and MVA pathway shapes isoprenoid metabolism in* C.
588 fairchildiana

589 The high isoprenoid emissions by *C. fairchildiana* offer a clue that might explain the
590 observed patterns in its $^{13}CO_2$ emissions. Among the four species we studied, only *C.*
591 *fairchildiana* emitted large amounts of isoprenoid VOCs, such as isoprene and monoterpenes,
592 including trans-β-ocimene (**Figure 3; Table 1**). Isoprene and monoterpenes are both
593 typically synthesized via the MEP pathway in the plastid (Dudareva *et al*., 2006). Previous
594 labeling studies have observed that cytosolic pyruvate is readily incorporated into MEP-
595 derived isoprenoids, typically with greater ^{13}C-enrichment from ^{13}C2-pyruvate than from
596 ^{13}C1-pyruvate (Fasbender *et al*., 2018; Yáñez-Serrano *et al*., 2019; Werner *et al*., 2020). This
597 is most likely due to the decarboxylation of pyruvate when it reacts with GA-3-P in the MEP
598 pathway, as the C2 carbon from pyruvate will be conserved while the C1 carbon is released
599 as CO_2 (**Figures 1, 8, step 4**) (Trapp and Croteau, 2001; Dudareva *et al*., 2004). However,
600 cytosolic pyruvate can also be converted to GA-3-P, which maintains all three carbons when
601 it enters the MEP pathway, providing a route for ^{13}C1-pyruvate to also create ^{13}C enriched
602 isoprenoids (**Figure 1, 8, step 2**) (Ladd *et al*., 2021).

603 In *C. fairchildiana*, isoprene was similarly enriched in ^{13}C whether it was labeled by
604 ^{13}C1- or ^{13}C2-pyruvate (**Figure 6**). This suggests that most of the isoprene that was
605 synthesized from the label used pyruvate that had been converted to GA-3-P. This could
606 partially explain the low ^{13}C enrichment of CO_2 respired by *C. fairchildiana* during labeling
607 with ^{13}C1-pyruvate, as all three carbons from the pyruvate label are conserved within the GA-
608 3-P derived isoprenoids, including non-volatile compounds that remained within the leaf.
609 Under drought conditions, *C. fairchildiana* isoprene emissions tended to decline (**Figure 3**),
610 but the ^{13}C enrichment of emitted isoprene during ^{13}C-pyruvate labeling increased (**Figure 6**).
611 This suggests that *de novo* synthesis of isoprene from primary photosynthate by *C.*
612 *fairchildiana* declined under drought as the availability of primary photosynthate also
613 declined, resulting in an increased proportion of the remaining isoprene flux being dependent
614 on cytosolic pyruvate via GA-3-P (**Figure 8, step 2-4**) (Souza *et al*., 2018; Yáñez-Serrano *et*
615 *al*., 2019).

616 Trans-β-ocimene emitted by *C. fairchildiana* was also ^{13}C enriched by both pyruvate
617 labels, but under pre-drought conditions it was more ^{13}C enriched from ^{13}C2-pyruvate than
618 ^{13}C1-pyruvate (**Figure 6**). Differing label incorporation patterns between these two

619 compounds were unexpected, since both compounds are derived from IPP and its isomer
620 dimethylallyl pyrophosphate (DMAPP) that are produced in the MEP pathway (**Figure 1,**
621 **step 4**). IPP and DMAPP are also produced in the cytosolic MVA pathway, where pyruvate
622 is incorporated only via acetyl-CoA, with the C1 position of pyruvate is decarboxylated prior
623 to their synthesis (**Figure 1, step 5**). Although exchange of these isoprenoid precursors across
624 the plastid membrane has long been suggested as metabolic crosstalk between the MEP and
625 MVA pathways (Arigoni *et al*., 1997; Hemerlin *et al*., 2003; Hemerlin *et al*., 2012), it
626 remains controversial due to a lack of proven IPP transporters (Rasulov *et al*., 2018; Souza *et*
627 *al*., 2018). However, transporters for geranyl pyrophosphate (GPP), an intermediate
628 compound between IPP and monoterpenes that can be produced in the cytosol (Bouvier *et al*.,
629 2001; Schmidt and Gerzhenzon, 2007; Zulak *et al*., 2010) as well as in the plastid, have been
630 identified (Bick and Lange, 2003; Gutensohn *et al*., 2012). The pattern of ^{13}C enrichment in
631 isoprenoids produced by *C. fairchildiana* during ^{13}C-pyruvate labeling in the pre-drought
632 period would be consistent with the transport of MVA derived GPP to the plastid, where it is
633 subsequently converted to monoterpenes that are only enriched by the ^{13}C2-pyruvate label.
634 The ^{13}C enrichment of trans-β-ocimene by ^{13}C1-pyruvate indicates synthesis through the
635 MEP pathway via GA-3-P, while the larger ^{13}C enrichment of trans-β-ocimene by ^{13}C2-
636 pyruvate indicates synthesis via MVA derived GPP as well as synthesis fully within the MEP
637 pathway. Isoprene, which is not synthesized from GPP, on the other hand, is ^{13}C enriched at
638 similar rates by both pyruvate labels since it is only sourced from MEP derived IPP/DMAPP.
639 During drought, trans-β-ocimene synthesis from MVA derived GPP apparently
640 declined or even completely shut down (**Figure 8, step 5**), as the ^{13}C-enrichment of β-
641 ocimene was similar from both ^{13}C1- and ^{13}C2-pyruvate, similar to isoprene (**Figure 6**). In
642 contrast to isoprene, ^{13}C enrichment of trans-β-ocimene declined with drought, indicating less
643 *de novo* synthesis of these compounds, even as *de novo* synthesis apparently became more
644 important for maintaining the isoprene flux (**Figure 6**). Despite the declining allocation of
645 carbon from the ^{13}C-pyruvate to trans-β-ocimene emissions, the rate of emission actually
646 increased with drought (**Table 1**). The enhanced trans-β-ocimene emissions under drought
647 thus may have been increasingly derived from storage pools (Lerdau *et al*., 1995, 1997;
648 Niinemets *et al*., 2002), diluting the ^{13}C enrichment of trans-β-ocimene during labeling.
649

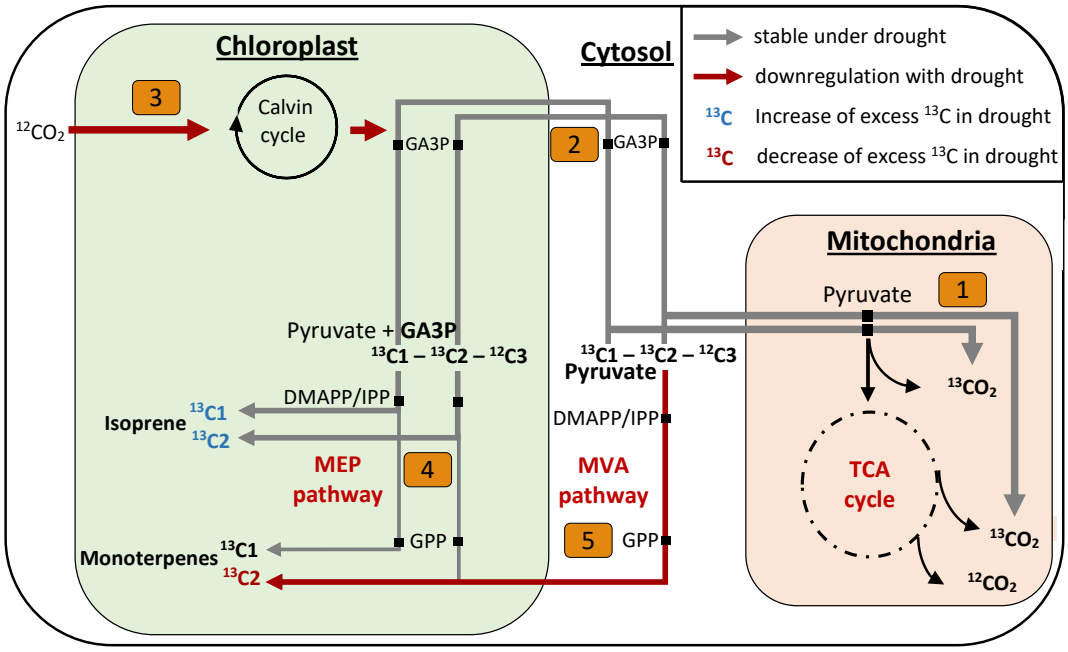

Figure 8: Schematic representation of pyruvate carbon partitioning among biosynthetic processes involved in the synthesis of isoprenoids and production of CO_2 within *Clitoria fairchildiana* cells as well as proposed adjustments of these processes during drought. Several intermediate steps and involved enzymes are removed for clarity. Arrow thickness represents the relative amount of ^{13}C1-/ ^{13}C2-labeled pyruvate utilized for the indicated pathway during pre-drought conditions. Gray arrows indicate no changes in carbon utilization during drought while brown arrows indicate a down-regulation of the pathway. Blue colored ^{13}C1/^{13}C2 indicate an increase in excess ^{13}C emissions of isoprene or monoterpenes during drought, while red color indicates a decline in excess ^{13}C emissions. Numbers represent the relevant pathways discussed, with descriptions of pathways 1-5 described in the caption of Figure 1. TCA, tricarboxillic acid; GA-3-P, glyceraldehyde 3-phosphate; DMAPP Dimethylallyl pyrophosphate; IPP, isopentenyl pyrophosphate; MEP, methylerythritol phosphate; GPP, geranyl pyrophosphate; MVA, mevalonic acid.

Conclusions

We use position specific ^{13}C-pyruvate labeling to investigate leaf level metabolic processes before and during an artificially imposed drought in the Biosphere 2 tropical rainforest. Our results indicate that although the TCA cycle is inhibited during the day, daytime respiration is dominated by anabolic processes that can result in a large CO_2 flux, representing up to 10 % of the allocation of the central metabolite pyruvate (**Figure 4**). This respiratory flux can change with drought stress, due to lower availability of pyruvate from reduced assimilation, but also from reduced allocation of the pyruvate that is available to anabolic processes that decarboxylate pyruvate, as in the case for *P. auritum*, which tended to accumulate more soluble sugars as osmolytes (Huang *et al*., in review). For species that did not accumulate soluble sugars (*H. rosa sinensis* and *P. dioica*) (**Figure 7**), the TCA cycle contributed relatively more CO_2 to daytime respiration under drought, most likely due to

increased produced of amino acids to serve as osmolytes. The chemical composition of osmolytes may thus impact the sources of daytime CO_2 emissions from leaves experiencing drought.

By simultaneously monitoring ^{13}C-pyruvate incorporation into secondary metabolites such as isoprenoids, we can gain insights into other metabolic shifts occurring within the leaf. In particular, our results suggest that *C. fairchildiana*'s reduced isoprene emissions under drought are at least partially due to lower substrate availability from lower photosynthetic activity. Additionally, the different patterns of label incorporation into isoprene and the monoterpene trans-β-ocimene illustrates linkages between the two pathways for isoprenoid biosynthesis, and adds to a growing body of evidence that GPP transport across the plastid membrane is more important than IPP transport for providing metabolic flexibility in isoprenoid production (**Figure 8**) (Bick and Lange, 2003; Gutensohn *et al*., 2012; Ladd *et al*., 2021). Overall, our results demonstrate that metabolic plasticity in response to drought can affect daytime respiratory processes and isoprenoid synthesis.

Acknowledgements: This study took place within the context of the B2WALD campaign, and was supported by the wider efforts of the entire B2WALD team, as described on the team contribution list (https://doi.org/10.25422/azu.data.14632662). We are particularly grateful to Michael Burman, Marissa Clover, Sydney Kerman, and Luke Miller for their assistance with leaf labeling in the forest canopy.

Author Contributions: Conceptualization (CW, SNL, LED); Data curation (LED, IB, JVH, LKM), Formal analysis (LED, SNL, JK, IB, AK, JVH, GP); Funding acquisition (CW, LKM); Investigation (SNL, LED, IB, JD, JVH, GP, JI, CW, AK); Methodology (CW, JK, IB, LED, SNL); Project administration (CW, SNL); Resources (CW, JVH, LKM); Supervision (CW, LKM, SNL); Validation (AK, CW, IB, LED, SNL); Visualization (LED, SNL); Writing – original draft (SNL, LED); Writing – review & editing: all.

Conflicts of interest: The authors declare no conflicts of interest.

Funding: This research was funded by the European Research Council (ERC consolidator grant 647008 to CW) and financial support from the Philecology Foundation to Biosphere 2 (obtained by LKM).

Data availability: All data included in this study will be published in the University of Arizona Research Data Repository. The DOI with the final data set will be included in the final version of the paper.

References:

Anjum SA, Xie XY, Wang LC, Saleem MF, Man C, Lei W. 2011. Morphological, physiological and biochemical responses of plants to drought stress. African Journal of Agricultural Research 6, 2026-2032.

Arigoni D, Sagner S, Latzel C, Eisenreich W, Bacher A, Zenk MH. 1997. Terpenoid biosynthesis from 1-deoxy-D-xylulose in higher plants by intramolecular skeletal rearrangement. Proceedings of the National Academy of Sciences of the United States of America 94, 10600-10605.

Atkin OK, Millar AH, Gardeström P, Day DA. 2000. Photosynthesis, carbohydrate metabolism and respiration in leaves of higher plants. In: Leegood RC, Sharkey TD, von Caemmerer S, eds. Photosynthesis. Photosynthesis and Respiration, vol. 9. Dordrecht: Springer, 153-175.

Bhargava S, Sawant K. 2013. Drought stress adaptation: metabolic adjustment and regulation of gene expression. Plant Breeding 132, 21-32.

Bick JA, Lange BM. 2003. Metabolic cross talk between cytosolic and plastidial pathways of isoprenoid biosynthesis: unidirectional transport of intermediates across the chloroplast envelope membrane. Archives of Biochemistry and Biophysics 415, 146-154.

Bouvier F, Suire C, D'Harlingue A, Backhaus RA, Camara B. 2001. Molecular cloning of geranyl diphosphate synthase and compartmentation of monoterpene synthesis in plant cells. The Plant Journal 24, 241-252.

Delauney AJ, Verma DPS. 1993. Proline biosynthesis and osmoregulation in plants. The Plant Journal 4, 215-223.

Dudareva N, Pichersky E, Gershenzon J. 2004. Biochemistry of plant volatiles. Plant Physiology 135, 1893-1902.

Dudareva N, Negre F, Nagegowda DA, Orlova I. 2006. Plant volatiles: recent advances and future perspectives. Critical Reviews in Plant Sciences 25, 417-440.

Farooq M, Hussain M, Wahid A, Siddique KHM. 2012. Drought stress in plants: An Overview. In: Aroca R, ed. Plant responses to drought stress. Berlin: Springer, 1-33.

Fasbender L, Yáñez-Serrano AM, Kreuzwieser J, Dubbert D, Werner, C. 2018. Real-time carbon allocation into biogenic volatile organic compounds (BVOCs) and respiratory carbon dioxide (CO_2) traced by PTR-TOF-MS, $^{13}CO_2$ laser spectroscopy and ^{13}C-pyruvate labelling. PLOS One 13, e0204398.

Ghirardo A, Gutknecht J, Zimmer I, Brüggemann N, Schnitzler J-P. 2011. Biogenic volatile organic compound and respiratory CO_2 emissions after ^{13}C-labeling: online tracing of C translocation dynamics in poplar plants. PloS One 6, e17393.

Guenther A, Hewitt CN, Erickson D, *et al*. 1995. A global model of natural volatile organic compound emissions. Journal of Geophysical Research: Atmospheres 100, 8873-8892.

Gutensohn M, Orlova I, Nguyen TTH, Davidovich-Rikanati R, Ferruzzi MG, Sitrit Y, Lewinsohn E, Pichersky E, Dudareva N. 2013. Cytosolic moterpene biosynthesis is supported by plastid-generated geranyl diphosphate substrate in transgenic tomato fruits. The Plant Journal 75, 351-363.

Haberstroh S, Kreuzwieser J, Lobo-do-Vale R, Caldeira MC, Werner C. 2018. Terpenoid emissions of two Mediterranean woody species in response to drought stress. Frontiers in Plant Science 9, 1071. doi: 10.3389/fpls.2018.01071

Harrison SP, Morfopoulos C, Srikanta Dani KG, *et al*. 2013. Volatile isoprenoid emissions from plastid to planet. New Phytologist 197, 49-57.

Hayes JM. 2004. An introduction to isotopic calculations. Woods Hole Oceanographic Institution, Woods Hole, MA, 2543.

Hemmerlin A, Hoeffler J-F, Meyer O, Tritsch D, Kagan IA, Grosdemange-Billiard C, Rohmer M, Bach TJ. 2003. Crosstalk between the cytosolic mevalonate and the plastidial methylerythritol phosphate pathways in tobacco bright yellow-2 cells. Journal of Biological Chemistry 278, 26666-26676.

Hemmerlin A, Harwood JL, Bach, TJ. 2012. A *raison d'être* for two distinct pathwys in the early steps of plant isoprenoid biosynthesis? Progress in Lipid Research 5, 95-148.

Heskel MA, Atkin OK, Turnbull MH, Griffin KL. 2013. Bringing the Kok effect to light: a review on the integration of daytime respiration and net ecosystem exchange. Ecosphere 4, 1-14.

Honeker L, Hildebrand G, Fudyma J, *et al*. 2021 Elucidating drought tolerance mechanisms in plant roots through 1H-NMR metabolomics, MALDI-MS, and NanoSIMS imaging technologies. Environmental Science & Technology 56, 2021-2032.

Jardine K, Wegener F, Abrell L, van Haren J, Werner C. 2014. Phytogenic biosynthesis and emission of methyl acetate. Plant, Cell & Environment 37, 414–424.

Ladd SN, Nelson DB, Bamberger I, Daber LE, Kreuzwieser J, Kahmen A, Werner C. 2021. Metabolic exchange between pathways for isoprenoid synthesis and implications for biosynthetic hydrogen isotope fractionation. New Phytologist 231, 1708-1719.

Lerdau M, Matson P, Fall R, Monson R. 1995. Ecological controls over monoterpene emissions from Douglas fir (*Pseudotsuga menziesii*). Ecology 76, 2640-2647.

Lerdau M, Guenther A, Monson R. 1997. Plant production and emission of volatile organic compounds. BioScience 47 6, 373-383.

Materić D, Bruhn D, Turner C, Morgan G, Mason N, Gauci V. 2015. Methods in plant foliar volatile organic compounds research. Applications in Plant Sciences 3, 1500044.

Metcalfe DB, Meir P, Aragao LEOC, Lobo-do-Vale R, *et al.* 2010. Shifts in plant respiration and carbon use efficiency at a large-scale drought experiment in the eastern Amazon. New Phytologist 187, 608-621.

Monson RK, Fall R. 1989. Isoprene emissions from aspen leaves: influence of environment and relation to photosynthesis and photorespiration. Plant physiology 90, 267-74.

Nayyar H, Kaur R, Kaur S, Singh R. 2014. γ-Aminobutyric acid (GABA) imparts partial protection from heat stress injury to rice seedlings by improving leaf turgor and upregulating osmoprotectants and antioxidants. Journal of Plant Growth Regulation 33, 408-419.

Niinemets Ü, Reichstein M. (2002). A model analysis of the effects of nonspecific monoterpenoid storage in leaf tissues on emission kinetics and composition in Mediterranean sclerophyllous Quercus species. Global Biogeochemical Cycles 16, 57–1.

Niinemets, Ü. 2010. Mild versus severe stress and BVOCs: thresholds, priming and consequences. Trends in Plant Science 15, 145–153.

O'Leary BM, Asao S, Miller AH, Atkin OK. 2019. Core principles which explain variation in respiration across biological scales. New Phytologist 222, 670-686.

Peñuelas J, Staudt M. 2010. BVOCs and global change. Trends in Plant Science 15, 133-144.

Pinheiro C, Chaves MM. 2011. Photosynthesis and drought: can we make metabolic connections from available data? Journal of experimental botany 62, 869-882.

Priault P, Wegener F, Werner C. 2009. Pronounced differences in diurnal variation of carbon isotope composition of leaf respired CO_2 among functional groups. New Phytologist, 181, 400-412.

Rascher U, Bobich EG, Lin GH, *et al.* 2004. Functional diversity of photosynthesis during drought in a model tropical rainforest - the contributions of leaf area, photosynthetic electron transport and stomatal conductance to reduction in net ecosystem carbon exchange. Plant, Cell & Environment 27, 1239-1256.

Rasmussen RA. 1970. Isoprene: Identified as a forest-type emission in the atmosphere. Environmental Science and Technology 4, 667-671.

Rasulov B, Talts E, Bichele I, Niinemets Ü. 2018. Evidence that isoprene emission is not limited by cytosolic metabolites. Exogenous malate does not invert the reverse sensitivity of isoprene emission to high [CO_2]. Plant Physiology 176, 1573-1586.

Reddy AR, Chaitanya KV, Vivekanandan M. 2004. Drought-induced responses of photosynthesis and antioxidant metabolism in higher plants. Journal of Plant Physiology 161, 1189-1202.

Rosolem R, Shuttleworth WJ, Zeng X, Saleska SR, Huxman TE. 2010. Land surface modeling inside the Biosphere 2 tropical rain forest biome. Journal of Geophysical Research Atmospheres 115, doi: 10.1029/2010JG001443

Schimel D, Pavlick R, Fisher JB, Asner GP, Saatchi S, Townsend P, Miller C, Frankenberg C, Hibbard K, Cox P. 2015. Observing terrestrial ecosystems and the carbon cycle from space. Global Change Biology 21, 1762-1776.

Schmitt A, Gershenzon J. 2007. Cloning and characterization of isoprenyl diphosphate synthases with farnesyl diphosphate and geranylgeranyl diphosphate synthase activity from Norway spruce (*Picea abies*) and their relation to induced oleoresin formation. Phytochemistry 68, 2649-2659.

Schuhr CA, Radykewicz T, Sagner S, Latzel C, Zenk MH, Arigoni D, Bacher A, Rohdich F, Eisenreich W. 2003. Quantitative assessment of crosstalk between the two isoprenoid biosynthesis pathways in plants by NMR spectroscopy. Phytochemistry Reviews 2, 3-16

Shinozaki K, Yamaguchi-Shinozaki K. 1998. Molecular responses to drought stress. In: Satoh K, Murata N, (eds). Stress responses of photosynthetic organisms. Amsterdam: Elsevier Science, 149-163

Souza VF, Niinemets Ü, Rasulov B, Vickers CE, Duvoisin Júnior S, Araújo WL. Concalves JFC. 2018. Alternative carbon sources for isoprene emission. Trends in Plant Science 23, 1081-1101.

Sweetlove LJ, Williams TCR, Maurice Cheung CY, Ratcliffe RG. 2013. Modelling metabolic CO_2 evolution – a fresh perspective on respiration. Plant, Cell & Environment 36, 1631-1640.

Tcherkez G, Cornic G, Bligny R, Gout E, Ghashghaie J. 2005. In vivo respiratory metabolism of illuminated leaves. Plant Physiology 138, 1596-1606.

Tcherkez G, Bligny R, Gout E, Mahé A, Hodges M, Cornic G. 2008. Respiratory metabolism of illuminated leaves de- pends on CO2 and O2 conditions. Proceedings of the National Academy of Sciences of the United States of America 105, 797–802.

Tcherkez G, Gauthier P, Buckley TN, *et al.* 2017. Leaf day respiration: low CO 2 flux but high significance for metabolism and carbon balance. *New Phytologist* 216, 986-1001.

Tcherkez G, Boex-Fontvieille E, Mahé A, Hodges M. 2012. Respiratory carbon fluxes in leaves. Current Opinion in Plant Biology 15 308-314.

Trapp S, Croteau R. 2001. Defensive resin biosynthesis in conifers. Annual Review of Plant Biology 52, 689-724.

von Caemmerer S, Farquhar GD. 1981. Some relationships between the biochemistry of photosynthesis and the gas exchange of leaves. Planta 153, 376-387.

Wehr R, Munger JW, McManus JB, Nelson DD, Zahniser MS, Davidson EA, Wofsy SC, Saleska SR. 2016. Seasonality of temperate forest photosynthesis and daytime respiration. Nature 534, 680-683.

Wegener F, Beyschlag W, Werner C. 2010. The magnitude of diurnal variation in carbon isotopic composition of leaf dark respired CO_2 correlates with the difference between $\delta^{13}C$ of leaf and root material. Functional Plant Biology 37, 849-858.

Werner C, Wegener F, Unger S, Nogués S, Priault P. 2009. Short-term dynamics of isotopic composition of leaf respired CO_2 upon darkening: measurements and implications. Rapid Communications in Mass Spectrometry 23, 2428–2438.

Werner C, Fasbender L, Romek KM, Yáñez-Serrano AM, Kreuzwieser, J. 2020. Heat waves change plant carbon allocation among primary and secondary metabolism altering CO_2 assimilation, respiration, and VOC emissions. Frontiers in Plant Science 11, 1242.

Werner C, Meredith LK, Ladd SN, *et al.* 2021. Ecosystem fluxes during drought and recovery in an experimental forest. Science 374, 1514-1518.

Yáñez-Serrano AM, Fasbender L, Kreuzwieser J, Dubbert D, Haberstroh S, Lobo-do-Vale R. Caldeira MC, Werner C. 2018. Volatile Diterprene emission by two Mediterranean *Cistaceae* shrubs. Scientific Reports 8, 6855.

Yáñez-Serrano AM, Mahlau L, Fasbender L, Byron J, Williams J, Kreuzwieser J, Werner C. 2019. Heat stress increases the use of cytosolic pyruvate for isoprene biosynthesis. Journal of Experimental Botany 70, 5827-5838.

Zhao J, Hartmann H, Trumbore S, Ziegler W, Zhang Y. 2013. High temperature causes negative whole-plant carbon balance under mild drought. New Phytologist 200, 330-339.

Zulak KG, Bohlmann, J. 2010. Terpenoid biosynthesis and specialized vascular cells of conifer defense. Journal of Integrative Plant Biology 52, 86-97.

Tables:

Table 1: Fluxes of common monoterpenes emitted by *q* as determined by GC-MS analysis of cartridge samples. Fluxes are reported as mean and standard error. [1]These two compounds co-eluted on the GC and the combined flux is reported.

	Pre-drought flux (pmol m^{-2} s^{-1})		Drought flux (pmol m^{-2} s^{-1})	
α-pinene	6.51	± 2.41	3.09	± 0.20
d-3-carene/ β-pinene[1]	9.28	± 2.96	5.52	± 0.46
limonene	5.10	± 0.79	4.39	± 0.23
trans-β-ocimene	5.47	± 1.20	28.88	± 7.35

Figure captions:

Figure 1: Schematic representation of important processes for the synthesis of isoprenoids and production of CO_2 within plant cells, with several intermediate steps removed for clarity. Green arrows represent possible movement of carbon from the C1 position of pyruvate and purple arrows represent movement of carbon from the C2 position of pyruvate. Numbers represent the relevant pathways discussed. 1: Transport of pyruvate into mitochondria, followed by initial decarboxylation of the C1-position and entrance into the TCA-cycle (i.e., catabolic respiration). 2: Conversion of pyruvate to GA-3-P and transport into the chloroplast. Pyruvate might also be transported directly to the chloroplast. All carbon positions of pyruvate remain in both cases. 3: Entrance of CO_2 into the Calvin cycle and addition of GA-3-P and other assimilation products into the metabolic pool of the chloroplast. 4: Initial reaction of pyruvate and GA-3-P to form DMAPP and IPP via MEP pathway, followed by reaction of two DMAPP/IPP molecules to produce GPP. As GA-3-P is not decarboxylated in this reaction, all carbon positions of the converted GA-3-P remain in the produced isoprene and monoterpenes. Pyruvate on the other hand is decarboxylated, resulting in only the C2-position remaining in these products 5: Entrance of pyruvate into MVA pathway and initial decarboxylation (i.e., anabolic respiration) of the C1-position of pyruvate to form DMAPP, IPP and subsequently GPP in the cytosol. After transport of these metabolites incorporating the ^{13}C2-label into the chloroplast, DMAPP and IPP can either enter isoprene or monoterpene synthesis, while GPP is utilized to synthesize monoterpenes. TCA, tricarboxlic acid; GA-3-P, glyceraldehyde 3-phosphate; DMAPP Dimethylallyl pyrophosphate; IPP, isopentenyl pyrophosphate; MEP, methylerythritol phosphate; GPP, geranyl pyrophosphate; MVA, mevalonic acid.

Figure 2: Representative leaves (panel a) and rates of (b) carbon assimilation, (c) transpiration, and (d) instantaneous water use efficiency measured on individual leaves of *Clitoria fairchildiana*, *Piper auritum, Hibiscus rosa sinensis*, and *Phytolacca dioica* under pre-drought (green) and drought (brown) conditions. Boxes represent the median and 25 – 75 % range of 7-12 replicate leaves. Whiskers and outliers calculated using Tukey's method. Significant differences between pre-drought and drought conditions for each species are indicated as * when $p < 0.05$, ** when $p < 0.01$, and *** when $p < 0.001$.

Figure 3: Emission rates of (a) isoprene and (b) monoterpenes measured on individual leaves of *Clitoria fairchildiana*, *Piper auritum, Hibiscus rosa sinensis*, and *Phytolacca dioica* under

pre-drought (green) and drought (brown) conditions. Fluxes from *C. fairchildiana* are plotted on the left y-axis while all other species are plotted on the right y-axis. Boxes represent the median and 25 – 75 % range of 7-12 replicate leaves. Whiskers and outliers are calculated using Tukey's method. Significant differences between pre-drought and drought conditions for each species are indicated as: * when $p < 0.05$.

Figure 4 Percent of ^{13}C from (a) $^{13}C1$-labeled pyruvate and (b) $^{13}C2$-labeled pyruvate that was released as CO_2 due to day respiration by *Clitoria fairchildiana*, *Piper auritum, Hibiscus rosa sinensis*, and *Phytolacca dioica* under pre-drought (open symbols) and drought (closed symbols) conditions. Note that the y-axes differ between panels, which was necessary to distinguish changes in production of CO_2 from $^{13}C2$-labeled pyruvate, which are an order of magnitude lower than those from $^{13}C1$-labeled pyruvate.

Figure 5 ^{13}C enrichment of CO_2 from $^{13}C1$-labeled pyruvate (y-axis) plotted relative to ^{13}C enrichment of CO_2 from $^{13}C2$-labeled pyruvate (x-axis) during pre-drought (open symbols) and drought (closed symbols). Symbols represent mean values and error bars represent one standard deviation of 3 – 6 replicate leaves per species.

Figure 6: ^{13}C from ^{13}C-labeled pyruvate incorporation into VOCs from *Clitoria fairchildiana*. Panel (a) shows ^{13}C excess isoprene emissions relative to theoretical background levels for isoprene and (b) shows ^{13}C enrichment of the monoterpene trans-β-ocimene relative to unlabeled measurements during pre-drought (green) and drought (brown) conditions (4 – 6 replicates per treatment). Boxes represent the median and 25-75% range of 7-12 replicate leaves. Whiskers and outliers are calculated using Tukey's method.

Figure 7: Trends in response to drought by *C. fairchildiana*, *P. auritum*, *H. rosa sinensis*, and *P. dioica*, expressed as percent decrease (blue shades) or increase (brown shades) of the mean drought value relative to the mean pre-drought value. Black borders indicate measurements where the mean values were significantly different at the $p < 0.05$ level. [1] Data from Werner *et al*., 2021. [2] Data from Huang *et al*., in review.

Figure 8: Schematic representation of pyruvate carbon partitioning among biosynthetic processes involved in the synthesis of isoprenoids and production of CO_2 within *Clitoria*

fairchildiana cells as well as proposed adjustments of these processes during drought. Several intermediate steps and involved enzymes are removed for clarity. Arrow thickness represents the relative amount of ^{13}C1-/ ^{13}C2-labeled pyruvate utilized for the indicated pathway during pre-drought conditions. Gray arrows indicate no changes in carbon utilization during drought while brown arrows indicate a down-regulation of the pathway. Blue colored ^{13}C1/^{13}C2 indicate an increase in excess ^{13}C emissions of isoprene or monoterpenes during drought, while red color indicates a decline in excess ^{13}C emissions. Numbers represent the relevant pathways discussed, with descriptions of pathways 1-5 described in the caption of Figure 1. TCA, tricarboxillic acid; GA-3-P, glyceraldehyde 3-phosphate; DMAPP Dimethylallyl pyrophosphate; IPP, isopentenyl pyrophosphate; MEP, methylerythritol phosphate; GPP, geranyl pyrophosphate; MVA, mevalonic acid.

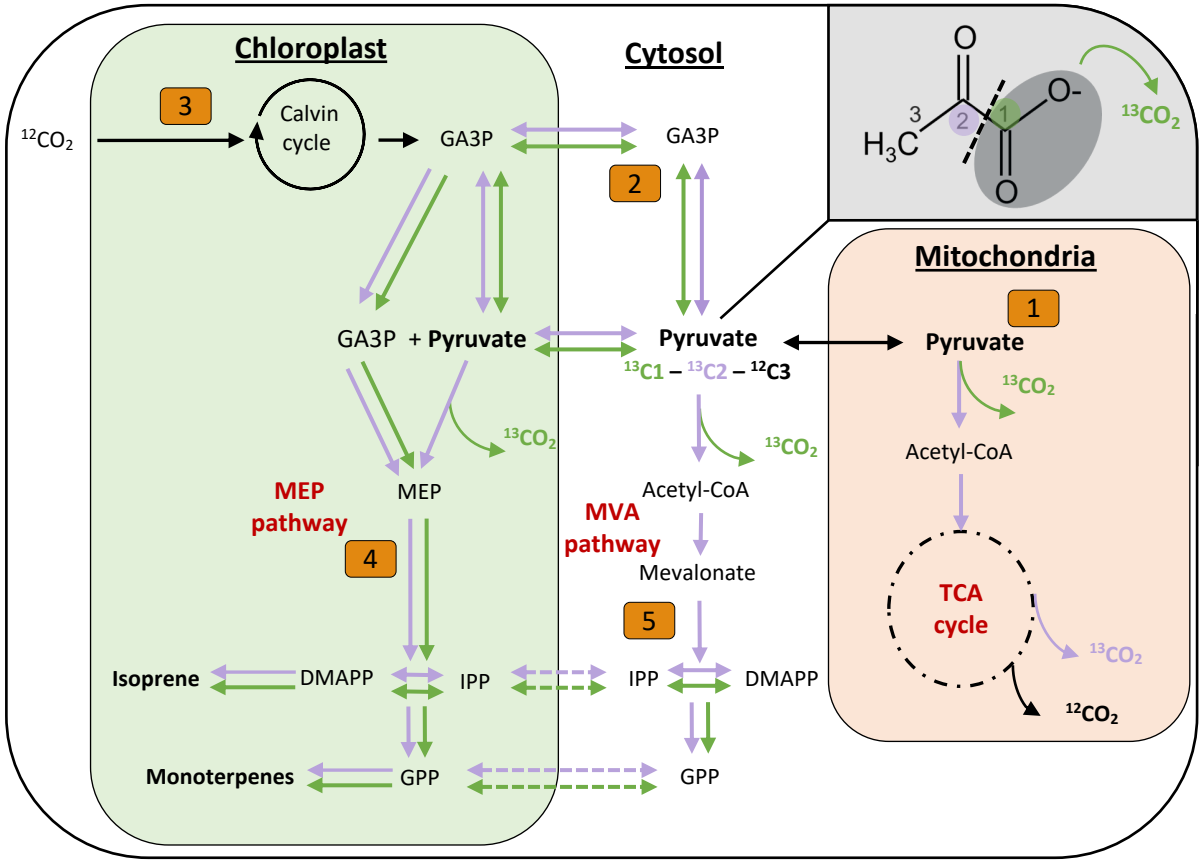
Chloroplast
Cytosol
Mitochondria
3
Calvin cycle
$^{12}CO_2$
GA3P
GA3P
2
GA3P + Pyruvate
Pyruvate
$^{13}C1 - ^{13}C2 - ^{12}C3$
$^{13}CO_2$
$^{13}CO_2$
MEP pathway
MEP
4
Acetyl-CoA
MVA pathway
Mevalonate
5
Isoprene
DMAPP
IPP
IPP
DMAPP
Monoterpenes
GPP
GPP
1
Pyruvate
$^{13}CO_2$
Acetyl-CoA
TCA cycle
$^{13}CO_2$
$^{12}CO_2$
O
O-
H_3C
3
2
1
O
$^{13}CO_2$

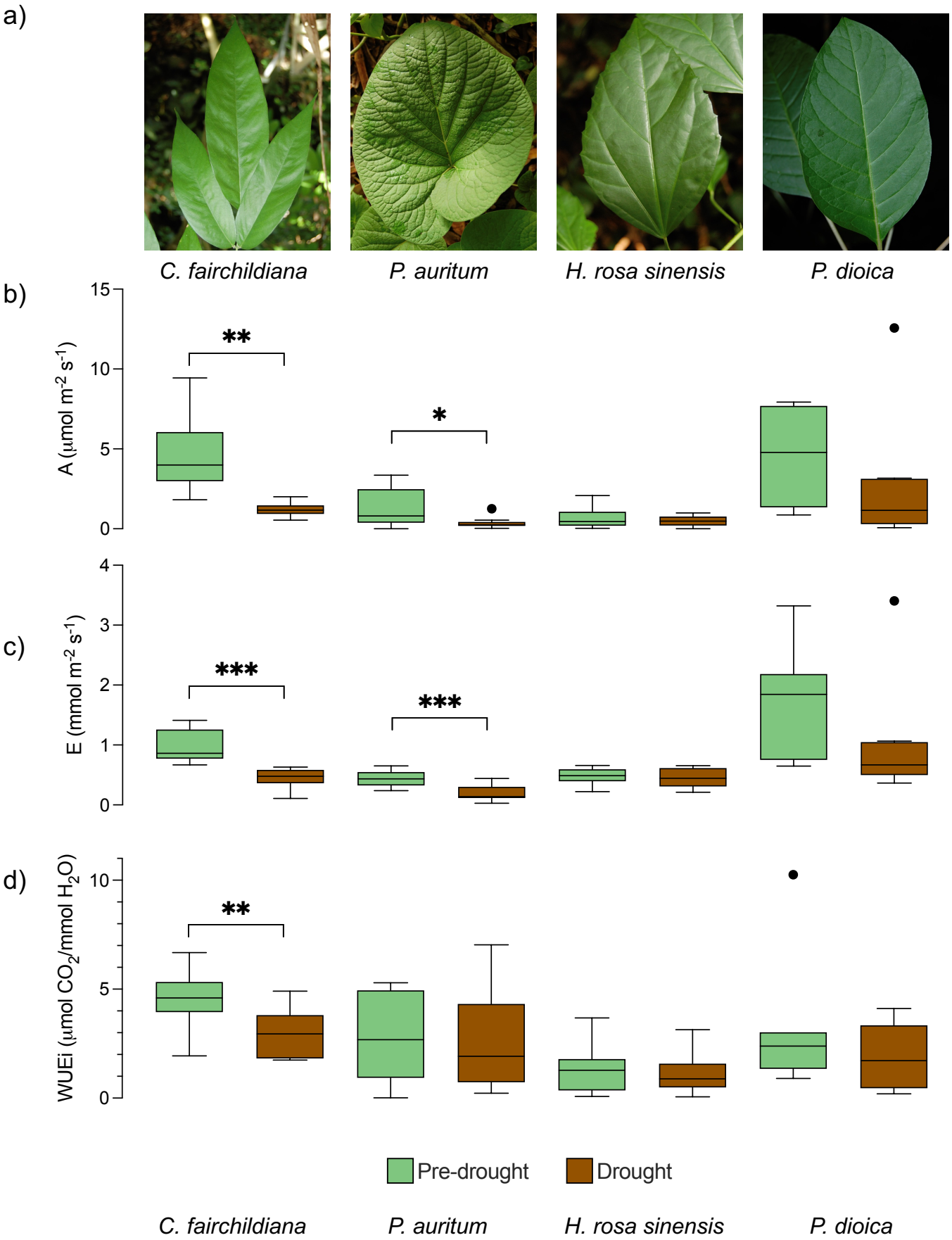
a)
C. fairchildiana
P. auritum
H. rosa sinensis
P. dioica
b)
A (µmol m-2 s-1)
15
10
5
0
**
*
c)
E (mmol m-2 s-1)
4
3
2
1
0
***
***
d)
WUEi (µmol CO2/mmol H2O)
10
5
0
**
Pre-drought
Drought
C. fairchildiana
P. auritum
H. rosa sinensis
P. dioica

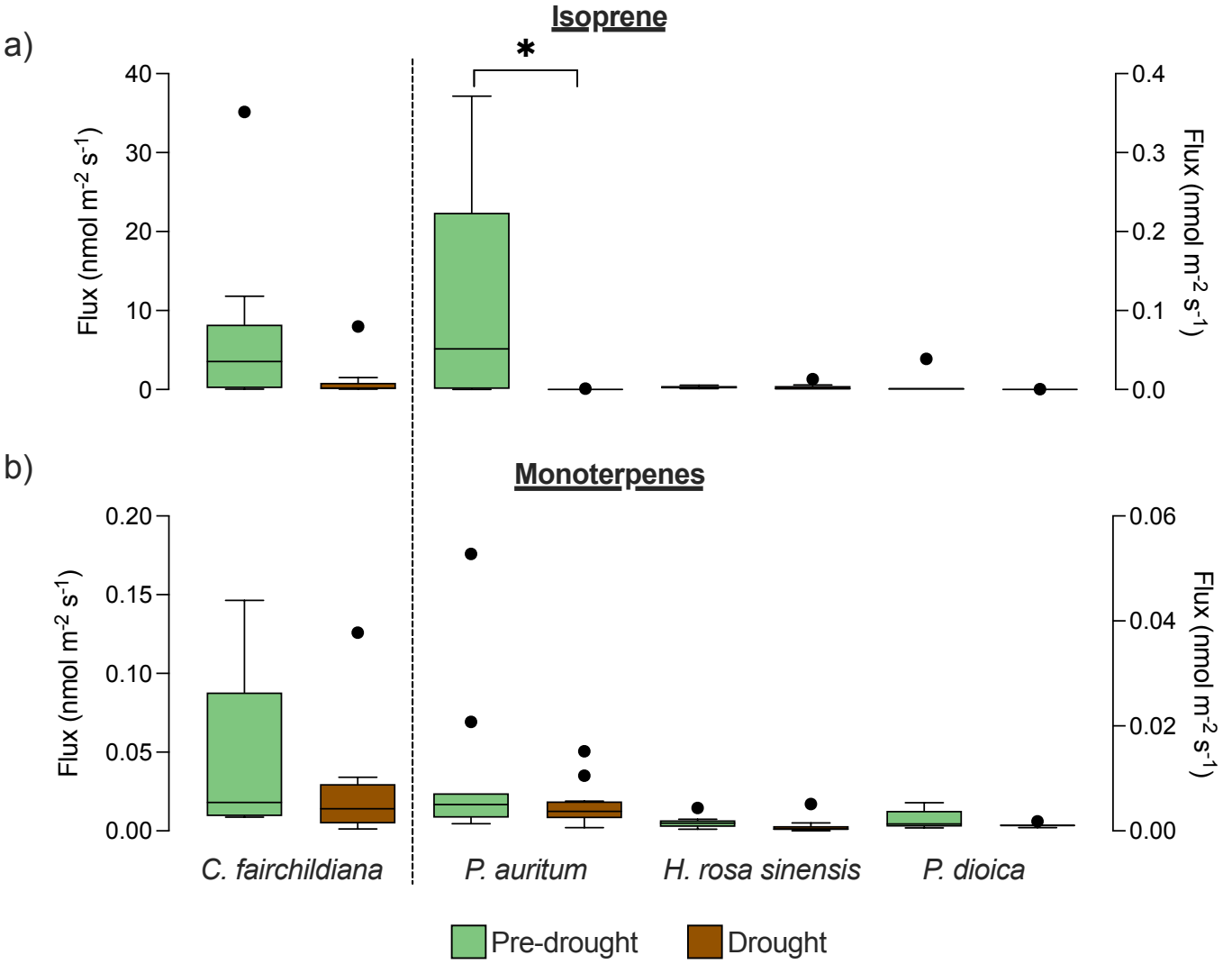
Isoprene
a)
*
Flux (nmol m-2 s-1)
40
30
20
10
0
0.4
0.3
0.2
0.1
0.0
Monoterpenes
b)
0.20
0.15
0.10
0.05
0.00
0.06
0.04
0.02
0.00
C. fairchildiana
P. auritum
H. rosa sinensis
P. dioica
Pre-drought
Drought

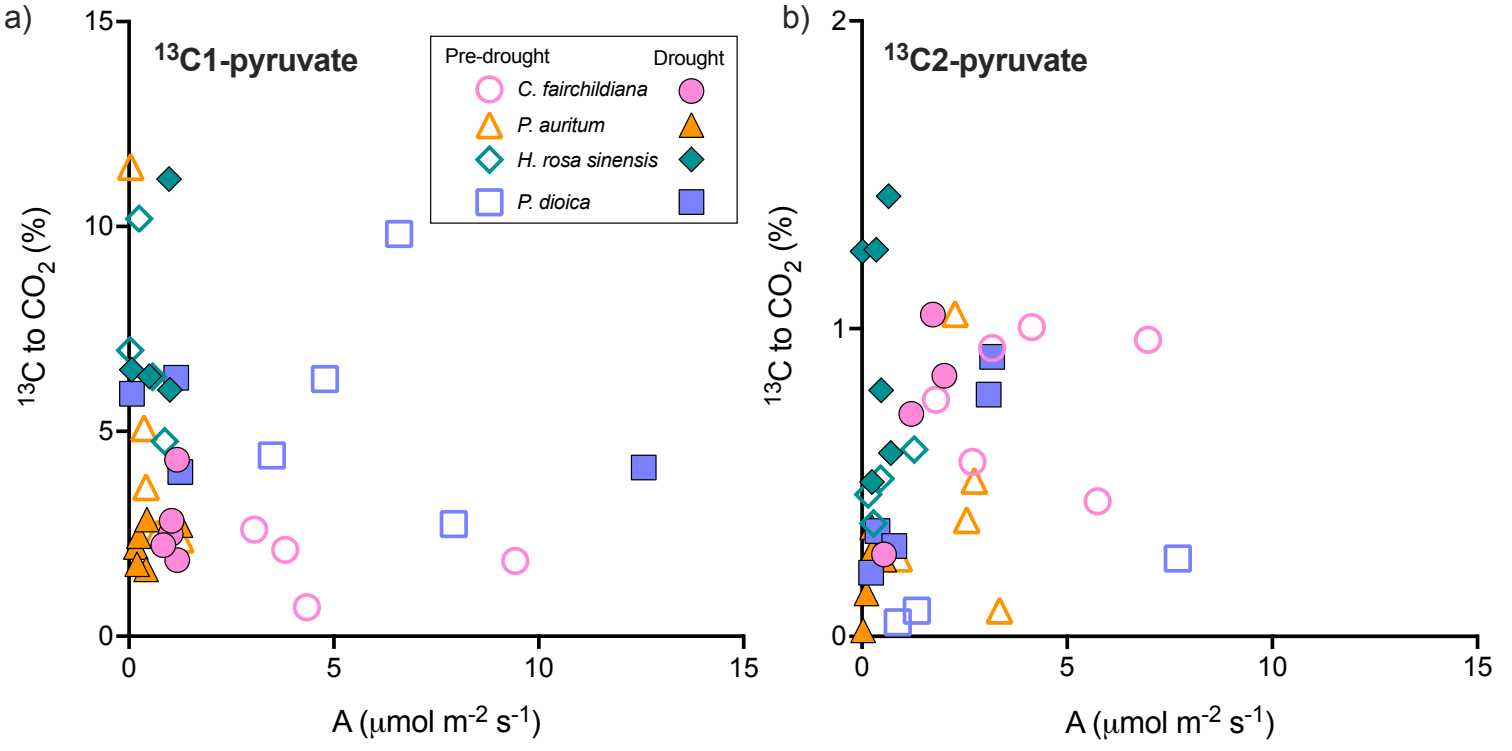
a)
^{13}C1-pyruvate
Pre-drought
Drought
C. fairchildiana
P. auritum
H. rosa sinensis
P. dioica
^{13}C to CO_2 (%)
A (μmol m^{-2} s^{-1})
0
5
10
15
b)
^{13}C2-pyruvate
^{13}C to CO_2 (%)
A (μmol m^{-2} s^{-1})
0
1
2
5
10
15

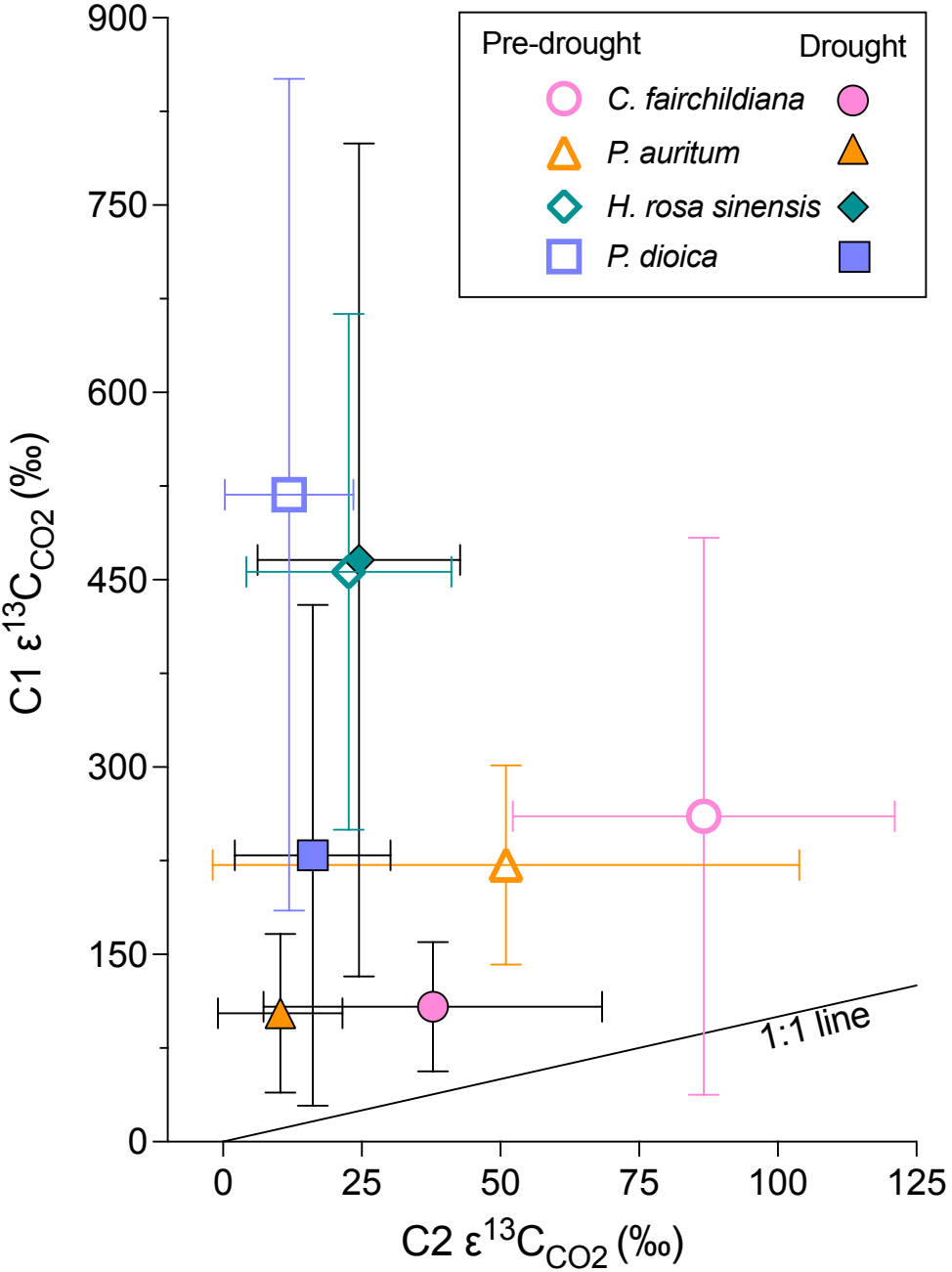
Pre-drought
Drought
C. fairchildiana
P. auritum
H. rosa sinensis
P. dioica
1:1 line
900
750
600
450
300
150
0
0
25
50
75
100
125
C1 ε13CCO2 (‰)
C2 ε13CCO2 (‰)

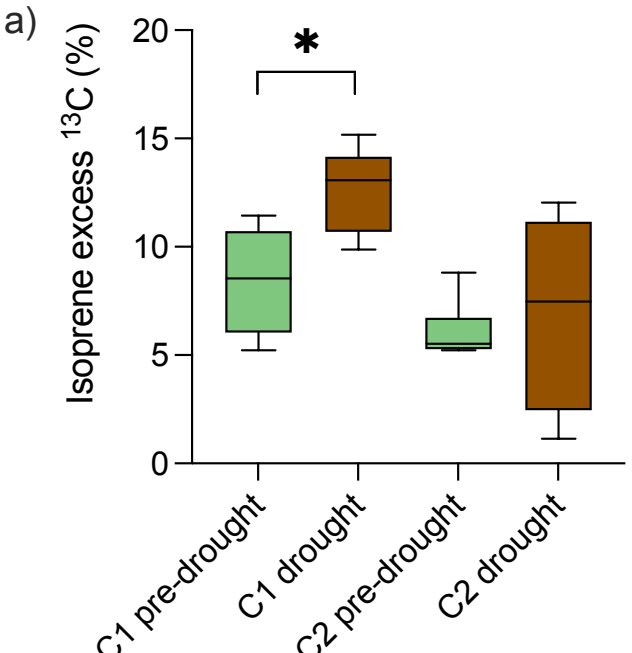
a)
Isoprene excess ^{13}C (%)
20
15
10
5
0
*
C1 pre-drought
C1 drought
C2 pre-drought
C2 drought

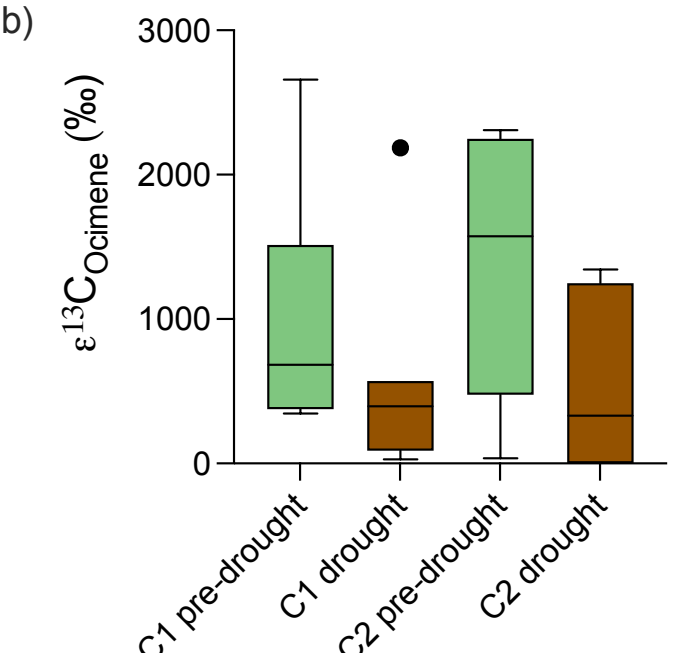
b)
$\varepsilon^{13}C_{Ocimene}$ (‰)
3000
2000
1000
0
C1 pre-drought
C1 drought
C2 pre-drought
C2 drought

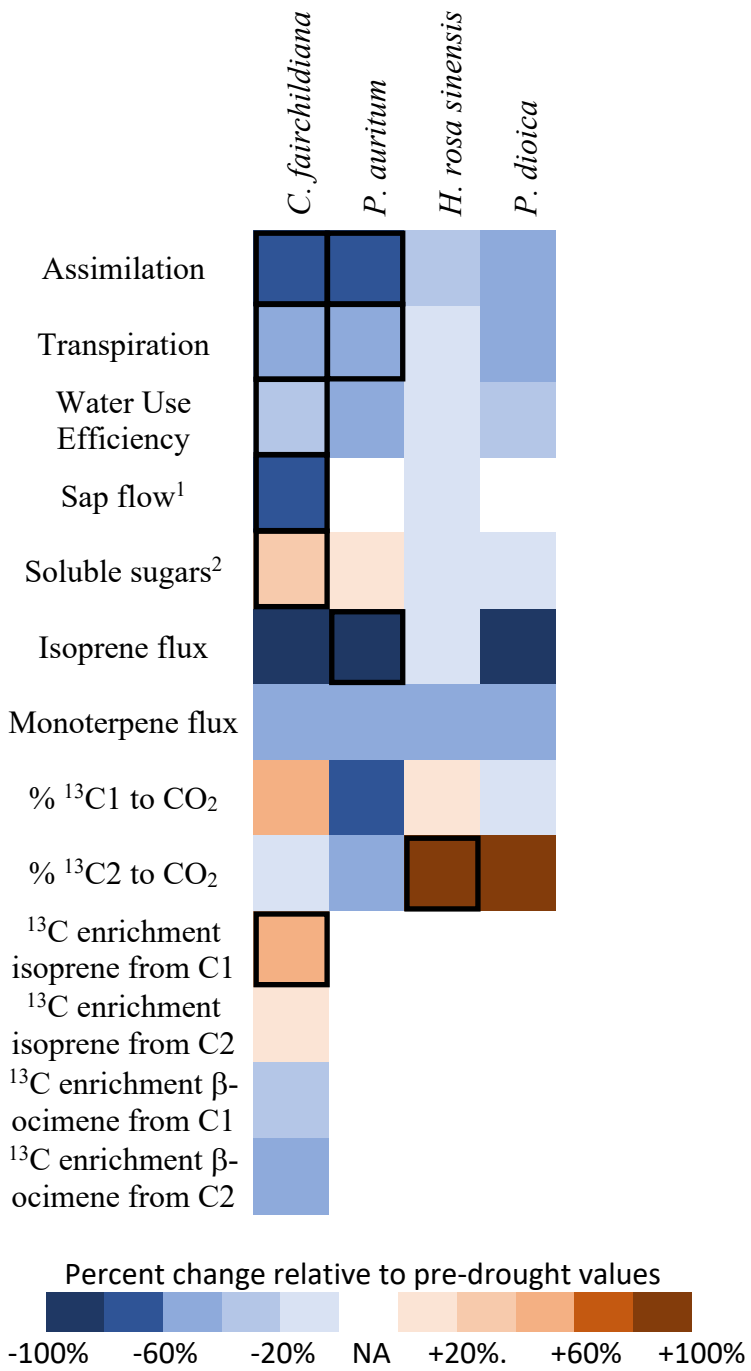
C. fairchildiana
P. auritum
H. rosa sinensis
P. dioica
Assimilation
Transpiration
Water Use Efficiency
Sap flow1
Soluble sugars2
Isoprene flux
Monoterpene flux
% 13C1 to CO2
% 13C2 to CO2
13C enrichment isoprene from C1
13C enrichment isoprene from C2
13C enrichment β-ocimene from C1
13C enrichment β-ocimene from C2
Percent change relative to pre-drought values
-100%
-60%
-20%
NA
+20%.
+60%
+100%

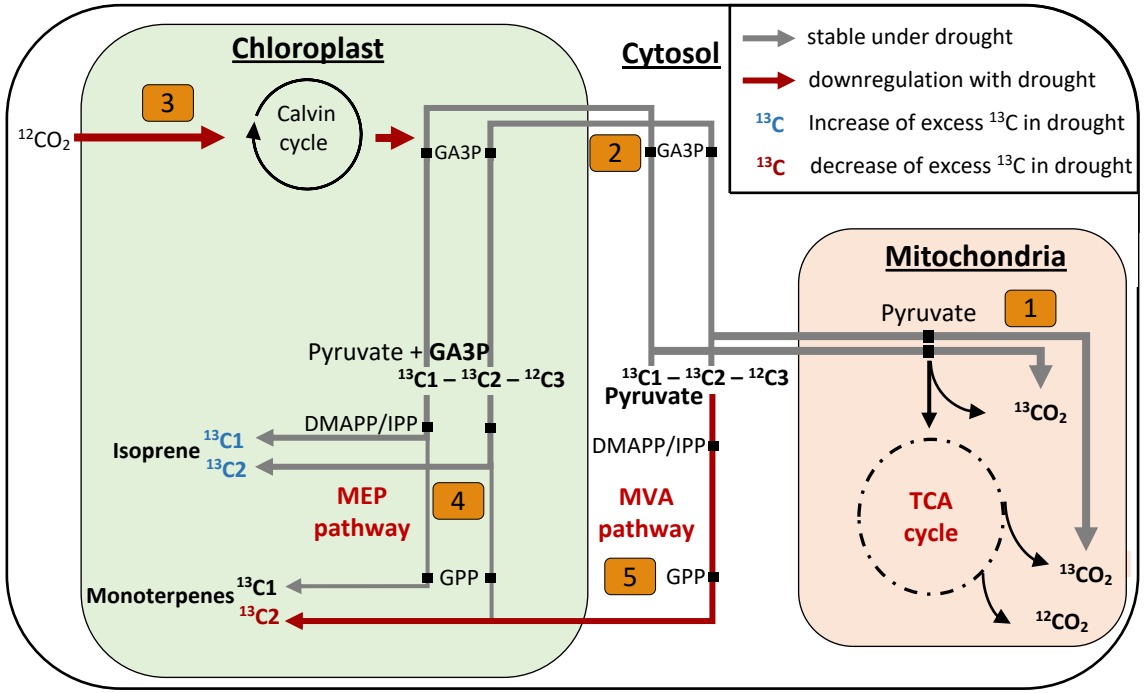
Chloroplast
Cytosol
Mitochondria
stable under drought
downregulation with drought
13C Increase of excess 13C in drought
13C decrease of excess 13C in drought
12CO2
3
Calvin cycle
GA3P
2
GA3P
Pyruvate + GA3P
13C1 – 13C2 – 12C3
13C1 – 13C2 – 12C3
Pyruvate
Pyruvate
1
13CO2
DMAPP/IPP
DMAPP/IPP
Isoprene
13C1
13C2
MEP pathway
4
MVA pathway
TCA cycle
13CO2
12CO2
GPP
5
GPP
Monoterpenes
13C1
13C2